A mean dynamic topography computed over the world ocean from altimetry, in situ measurements, and a geoid model

M.-H. Rio[1] and F. Hernandez

CLS Space Oceanography Division, Ramonville, France

Received 26 November 2003; revised 28 May 2004; accepted 12 October 2004; published 28 December 2004.

[1] The lack of an accurate geoid still prevents precise computation of the ocean absolute dynamic topography from satellite altimetry and only sea level anomalies (SLA) can be accurately deduced. In the new context of Global Ocean Data Assimilation Experiment (GODAE) where models are assimilating satellite altimetry, the estimation of a realistic mean dynamic topography (MDT) consistent with SLA is a crucial issue. In a first "direct" approach, a MDT is computed by subtracting the geoid model EIGEN-2 from the Mean Sea Surface Height CLS01, determined from 7 years of altimetric data (TOPEX and ERS1,2) at spherical harmonic degree 30. To provide the scales shorter than 660 km, the Levitus climatology is merged with the resulting MDT, both weighted by their respective errors. This solution provides a "first guess" for the computation of a global and higher resolution MDT. Then, a "synthetic" technique is used to combine in situ measurements and altimetric data: TOPEX and ERS1,2 altimetric anomalies are subtracted from in situ measurements of the full dynamical signal (based on buoy velocities from the WOCE-TOGA program and XBT, CTD casts). The resulting values provide local estimates of the mean field, in terms of currents or dynamic topography, which are used to improve the first guess using an inverse technique. The MDT obtained is compared to other mean dynamic fields, and a verification using independent in situ data shows improvements in most areas. It exhibits a more energetic representation of the subtropical and subpolar gyres; sea level gradients associated with the main currents are strongly enhanced. Differences with independent velocity observations are globally lower than 13 cm/s rms. *INDEX TERMS:* 4532 Oceanography: Physical: General circulation; 4512 Oceanography: Physical: Currents; 1640 Global Change: Remote sensing; *KEYWORDS:* altimetry, mean circulation, geoid

Citation: Rio, M.-H., and F. Hernandez (2004), A mean dynamic topography computed over the world ocean from altimetry, in situ measurements, and a geoid model, *J. Geophys. Res.*, *109*, C12032, doi:10.1029/2003JC002226.

1. Introduction

[2] Since the launch of the first altimetric satellites in the 1970s, altimetric data have been widely used by the oceanographic community in order to better understand the global oceanic system and its evolutions at various spatial and temporal scales [*Fu and Cazenave*, 2001]. However, still today, it is not possible to make direct use of altimetric signal for oceanographic circulation applications. Indeed, an altimeter measures with high precision and unique resolution the sea surface height (SSH) above a reference ellipsoid, whereas the signal of interest for oceanographers is the so-called dynamic topography (i.e., the sea level above the geoid). A geoid accuracy compatible with oceanic phenomena is thus required. Typically, important aspects of the oceanic circulation contain wavelengths as short as 100–200 km. Such a geoid accuracy is not achieved yet [*Nerem et al.*, 1994; *Rapp et al.*, 1996; *Stammer and Wunsch*, 1994], and the shortest scales will only be provided by the Gravity Field and Steady state Ocean Circulation Explorer (GOCE) mission (scheduled in 2007) that aims to measure the Earth's gravity field with centimetric precision at a 100-km resolution.

[3] To compensate for large geoid errors, altimetric mission repetitiveness was planned. By averaging over a given period P all altimetric heights η measured at a given location, one determines a "mean profile" of heights $\bar{\eta} = G + \bar{h}$, equal to the geoid G, which is supposed stationary over the chosen period, plus the mean dynamic topography $\bar{h}$. When subtracting $\bar{\eta}$ from a single altimetric measurement $\eta = G + h$, the geoid G is removed and the sea level anomalies (SLA) obtained, η' correspond to h', the variable part of the dynamic topography. This is the so-called repeat-track method that provides SLA with 3- to 4-cm accuracy.

[4] In the framework of the Enhanced Ocean Data Assimilation and Climate Prediction (ENACT) project, which was undertaken in line with the recommendations of the European climate research community (EUROCLIVAR, November 1998), and of the International CLIVAR programme, SLA are computed with respect to a 1993–

[1]Now at Istituto di Scienze dell'Atmosfera e del Clima—CNR, Rome, Italy.

0148-0227/04/2003JC002226

1999 mean profile and distributed to the oceanographic community. To reconstruct from these anomalies the absolute dynamic topography, an accurate estimate of the mean dynamic topography (MDT) for the 1993–1999 period is needed. Provided this is consistent with SLA, it will allow to determine globally the ocean absolute dynamic topography from all past and future altimetric missions. This is a crucial issue for the further understanding, modeling, and forecasting of the ocean circulation from mesoscale to global scale. In particular, it will significantly improve the oceanic transport estimation [*Ganachaud et al.*, 1997; *Le Provost et al.*, 1999; *LeGrand*, 2002; *LeGrand and Minster*, 1999]. Subsequently, it will provide better constraints for ocean general circulation models (OGCM). Also, the use of an accurate MDT will contribute to major improvements in data assimilating forecasting systems [*Le Provost et al.*, 1999; *Le Traon et al.*, 2002]. This is an important goal also in the context of the Global Ocean Data Assimilation Experiment (GODAE), which aims to set up operational ocean monitoring and forecasting systems on global scale (as MERCATOR (French component of GODAE), TOPAZ (Norwegian component), HYCOM (US component), and FOAM (UK component)) or on regional scales, as Mediterranean ocean Forecasting System (MFS).

[5] In order to retrieve precise absolute dynamic topography values from altimetry, various attempts were made to compute accurate local estimates of either the mean dynamic topography or the geoid. *Kelly and Gille* [1990] used a simple velocity profile model of the Gulf Stream (improved by *Qiu* [1992, 1994], who added a westward flowing recirculation to the main eastward flow) to estimate the MDT from GEOSAT SLA through an iterative method. The MDT obtained for the Gulf Stream was validated by *Kelly et al.* [1991] and *Joyce et al.* [1990] comparing the resulting GEOSAT dynamic topography values to hydrographic and acoustic Doppler current profiler (ADCP) data. A similar method was used by *Gille* [1994] to map the Antarctic Circumpolar Current. However, this method only applies to jet-like current regions.

[6] A synthetic geoid method was used by *Mitchell et al.* [1990], where absolute dynamic topography deduced from airborne expendable bathythermograph (AXBT) were subtracted from simultaneous GEOSAT altimeter SSH in order to provide along track estimates of the geoid. Similarly, *Glenn et al.* [1991] computed a MDT from 1 year of real-time forecasts and nowcasts of a dynamical model in the Gulf Stream area. Using a MSS determined over the same year using GEOSAT altimetric data, they estimated a geoid. This geoid was validated by *Porter et al.* [1992, 1996] comparing the resulting GEOSAT absolute dynamic topography to independent in situ measurements. *Feron et al.* [1998] proposed to derive a MDT from the average vorticity field as deduced from 3 years of GEOSAT SLA. The method was shown to be applicable only in strong mesoscale variability areas.

[7] None of these local methods were implemented globally. Various approaches exist to evaluate globally a MDT. The oldest solutions consist of climatologies computed from dynamic height compilations [*Levitus et al.*, 2001]. However, the large period covered by such a MDT (several decades) differs from the required period (e.g., 1993–1999) and results in very smooth solutions. Besides, being based on hydrographic data alone, they are defined relatively to an arbitrary level of no motion. A derived technique consists in using inverse modeling to estimate a full dynamic topography from hydrographic and/or Lagrangian data. Its formalism is described by *Mercier* [1986] and *Wunsch* [1978, 1996], and the method was used by (among others) *Ganachaud et al.* [1997], *Le Traon and Mercier* [1992], *Martel and Wunsch* [1993], *Mercier* [1989], and *Mercier et al.* [1993]. Recently, a global solution was computed by *LeGrand et al.* [2003] based on *Mercier et al.* [1993] inverse modeling. This technique allows us to prescribe the ocean dynamics (e.g., geostrophy), but it is still based on data gathered over several decades. Therefore the solutions are smooth and not consistent with the mean matching the altimetry averaging period. A third technique is to average over the required period outputs from an OGCM with or without assimilation of hydrographic data. The resulting MDT are limited by model bias and/or assimilation system errors. More accuracy is expected in the future with assimilation technique enhancement. In the meantime, methods were developed to improve a posteriori the obtained model means. *Ezer et al.* [1993] suggested various methods to reconstruct the MDT from model averages. *Ichikawa et al.* [1995] proposed an iterative correction of a model average by assimilating altimetric data and drifting buoys velocities. *Greiner* [2000] used a morphing technique based on sea surface temperature data applied to an original model-averaged MDT. Finally, the most direct method for estimating a global MDT consists in subtracting a geoid model from an altimetric mean sea surface (MSS). As we mentioned earlier, this direct solution is not valid yet at short scales due to significant geoid errors.

[8] The lack of a satisfying global solution to be used to reference altimetric anomalies motivated the present study. To estimate a global and accurate MDT, totally consistent with altimetric SLA, the three data types available (altimetric measurements, in situ data, and a geoid model) are combined according to the following three steps: First, altimetric data and the geoid model are combined through the already mentioned "direct method" (MSS minus geoid) whose principle and results are described in the second section of the present paper. Owing to geoid errors, this method allows to retrieve only the MDT's longest wavelengths. This information is used in section 3 to estimate a first guess of the required MDT. Then, altimetric data and in situ data were combined through the so-called "synthetic method" whose principle and results are described in section 4. The resulting local estimates of the required MDT are used in section 5 to improve the first guess computed in section 3. The combined mean dynamic topography (CMDT RIO03) obtained is validated in section 6. A summary of the results and main conclusions are given in section 7.

2. Combination of Altimetric Data and a Geoid Model: The Direct Method

2.1. Method

[9] The most direct method to estimate the mean dynamic topography for the required 1993–1999 period is to subtract a geoid model from the altimetric MSS over the same

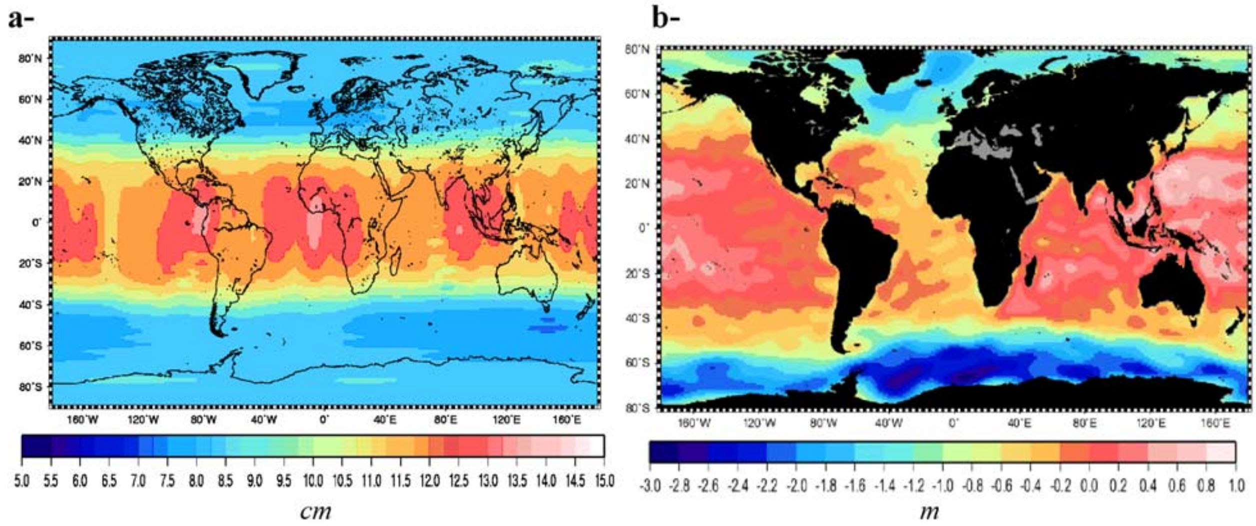

Figure 1. (a) Cumulated error at degree 30 for geoid model EIGEN2. (b) Mean dynamic topography obtained at degree 30 subtracting the EIGEN2 geoid from the mean sea surface CLS01.

period. We investigate here which wavelengths of the MDT can be accurately deduced from this so-called ‘‘direct method.’’ To implement the method, a filter is first applied to both the geoid model and altimetric MSS to retain only the spatial scales for which the geoid is accurate enough. For that purpose, the spherical harmonic coefficients are determined for both surfaces. A comprehensive description of spherical harmonic expansion theory is given by *Hobson* [1955]. When reconstructing the field using the coefficients up to a maximum degree lmax, only the wavelengths greater than 40,000 km/lmax are kept, corresponding to a spatial resolution equal to 20,000 km/lmax.

2.2. Data

2.2.1. Altimetric Mean Sea Surface

[10] The altimetric MSS CLS01 used here was computed over the required 1993–1999 period by *Hernandez et al.* [2001] using data from four satellites: GEOSAT, ERS1-2, and TOPEX/Poseidon. Mean heights were computed from 80°S to 82°N on a one-thirtieth degree regular grid with a smooth transition to the EGM96 geoid model on continental shelves. Formal error on the obtained field is globally less than 3 cm.

2.2.2. Geoid Model

[11] EGM96 is currently the only geoid resolving the shortest scales (down to 55 km). It was developed by the NASA Goddard Space Flight Center (GSFC) and the National Imagery and Mapping Agency (NIMA) using orbital perturbations from 40 satellites, in situ gravimetric measurements, and altimetric data [*Lemoine et al.*, 1998]. Owing to the inclusion of altimetric data, this model is not appropriate for the present study. Instead, we used the EIGEN-2 solution [*Reigber et al.*, 2003], which was computed by GRGS/GFZ integrating 6 months of CHAMP data to the previous GRIM5-s1 solution (based on orbital perturbation analyses [*Biancale et al.*, 2000]). Figure 1a gives the EIGEN-2 cumulated error at spherical harmonic degree 30 (i.e., spatial resolution of ~660 km) issued from a calibrated variance/covariance matrix (J.-M. Lemoine, personal communication, 2003). Stronger errors are obtained at middle and low latitudes (from 10 to 15 cm) than at high latitudes (lower than 10 cm): CHAMP orbit is quasipolar so that the satellite ground tracks are denser at high latitudes and the spatial resolution of the data is increased.

2.3. Results: The CLS01-EIGEN2 MDT

[12] From the degree 30 expansion of the CLS01 MSS and the EIGEN-2 geoid, a MDT at the same expansion is determined by subtraction (Figure 1b). The corresponding zonal and meridional velocities are deduced by geostrophy (Figure 2). The MDT obtained (hereinafter CLS01-EIGEN2 MDT) exhibits the basic features of the large-scale oceanic circulation with the Atlantic, Pacific, and South Indian subtropical gyres and intensified western boundary currents. The Gulf Stream, Kuroshio and Aghulas currents, as well as the Antarctic Circumpolar Current, display strong zonal velocities (15 to 25 cm/s). Strong cyclonic circulation is observed near 180°E, 60°S corresponding to the Weddell gyre. Similarly, in the Northern Hemisphere, strong cyclonic circulations are observed for the subpolar gyre, in the Greenland and Norway basins. Equatorial current systems are well marked in all basins. Equatorial and counter-equatorial currents exhibit strong zonal velocities (reaching ±40 cm/s). In the Pacific Ocean, strong positive zonal velocities (eastward currents) are obtained at 5°N–10°N corresponding to the North Equatorial Counter Current, and strong negative zonal velocities (westward currents) are obtained for the North Equatorial Current (20 cm/s) and South Equatorial Current (30–40 cm/s).

2.4. Comparison With a Modeled MDT

[13] In order to evaluate further the mean dynamic topography obtained by the ‘‘direct method,’’ we compare it to the mean dynamic topography obtained by averaging OCCAM model outputs at the same spatial resolution. The Ocean Circulation and Climate Advanced Modeling (OCCAM) project is a primitive equation model developed at Southampton Oceanography Centre in collaboration with East Anglia and Edinburgh universities [*Fox and Haines*,

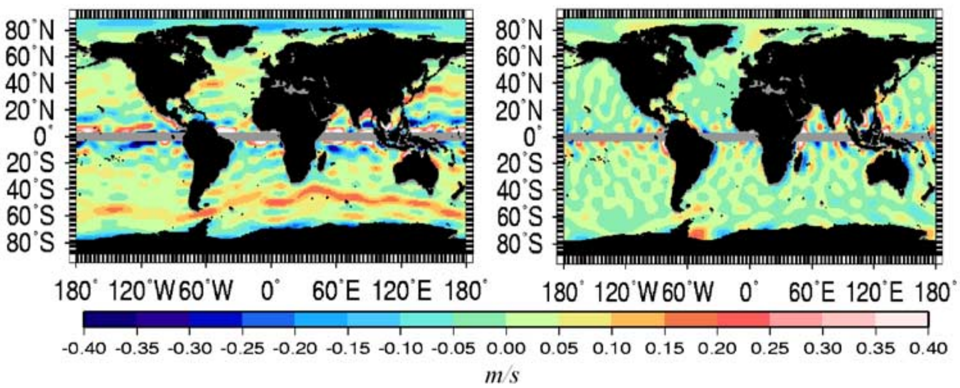

Figure 2. Geostrophic (left) zonal and (right) meridian velocities associated with the CLS01-EIGEN2 MDT.

2003]. The outputs of the simulation that assimilates XBT data [*Troccoli and Haines*, 1999] were time-averaged over the period 1993–1995. In order to proceed to comparable comparisons with the CLS01-EIGEN2 MDT (covering the 1993–1999 period), the OCCAM MDT was adjusted to the 1993–1999 mean (Figure 3). To do so, the average over the period 1993–1995 of the SLA (referenced to the 1993–1999 period) was subtracted from the initial OCCAM 1993–1995 mean. To compute spherical harmonic coefficients, the mean field is extrapolated over the continents. Scales shorter than 660 km are filtered out by reconstructing the mean field only to degree 30, like for the CLS01 MSS and EIGEN2 geoid. The total root mean square difference between the resulting OCCAM mean and the CLS01-EIGEN2 MDT is 22.3 cm. It is reduced to 13.3 cm RMS when considering only the latitudes equatorward of 40°. This value is consistent with the 10- to 15-cm geoid errors at these latitudes, although it also contains the errors on OCCAM mean. Consequently, the error on the EIGEN-2 geoid as given in Figure 1 might be slightly overestimated. Inversely, at high latitudes, both geoid errors and CLS01 MSS errors are low, suggesting that the higher mean height differences are rather due to OCCAM model uncertainties. Models are generally less precise at high latitudes due to large barotropic current errors, bad water mass initialization, or less accurate forcing fields.

[14] These results strengthen our belief that the direct method can be used to retrieve the longest wavelengths of the MDT, with higher confidence at high latitudes, where the error is expected to be less than 10 cm.

3. Construction of a MDT First Guess

[15] In order to provide a more accurate large-scale MDT than the CLS01-EIGEN2 solution, the mean heights deduced from the Levitus climatology referenced to 1500 dbar are included. As mentioned, climatology MDTs are smooth and partly miss the barotropic signal. However, a better precision than the CLS01-EIGEN2 is expected at low latitudes, where the baroclinic signal is dominant.

[16] The Levitus climatology referenced to 1500 m is not defined at depths shallower than 1500 m. To construct a global surface on a 1° resolution grid, we first extend the climatological heights toward the coast; step by step, for each grid point whose bathymetry is shallower than 1500 m, a geostrophic velocity is computed using the dynamic heights of the four adjacent grid points, defining the reference depth as the shallowest of the four points. Combining by multivariate objective analysis (see Appendix A) this set of velocities to the original Levitus MDT referenced to 1500 dbar, an extended climatology (ECMDT) is obtained, defined at all depths. As for the OCCAM MDT, the ECMDT scales shorter than 660 km are filtered out using the spherical harmonic expansion, and both ECMDT and CLS01-EIGEN2 MDT long wavelengths are then combined by objective analysis: ECMDT heights are corrected by CLS01-EIGEN2 MDT heights sampled every 5° (such a resolution is allowed by the long wavelengths considered here), whose error level is given by the geoid accuracy (see Figure 1), neglecting the CLS01 MSS error at those wavelengths. Errors for both the geoid and the climatology allow an optimal weighting on the two sets of information. The resulting surface stays close to the ECMDT long wavelengths at low and middle latitudes, where it is assumed to be accurate, and geoid errors are large, while high latitudes are constrained by the CLS01-EIGEN2 heights, where Levitus climatology is less accurate. Finally, we add back the shortest scales extracted from the ECMDT to the surface estimated above, so as to obtain the MDT first guess (Figure 4). It exhibits a strong Antarctic Circumpolar Current as well as marked subpolar gyres (south in the Weddell Sea and north in the Irminger, Greenland, and Norway basins). Also, the Aghulas current is intensified with respect to the initial Levitus climatology's pattern, and an important anticyclonic recirculation cell is observed.

4. Combination of Altimetric Data and In Situ Data: The Synthetic Method

4.1. Method

[17] The synthetic method alternatively allows to estimate locally the required MDT by subtracting the oceanic variability as observed by altimetry from in situ measurements of the absolute oceanographic signal. At a time t_1 and position r_1, where an in situ measurement h of the ocean dynamic topography and a simultaneous altimetric SLA h'_a are available (with associated measurement errors respec-

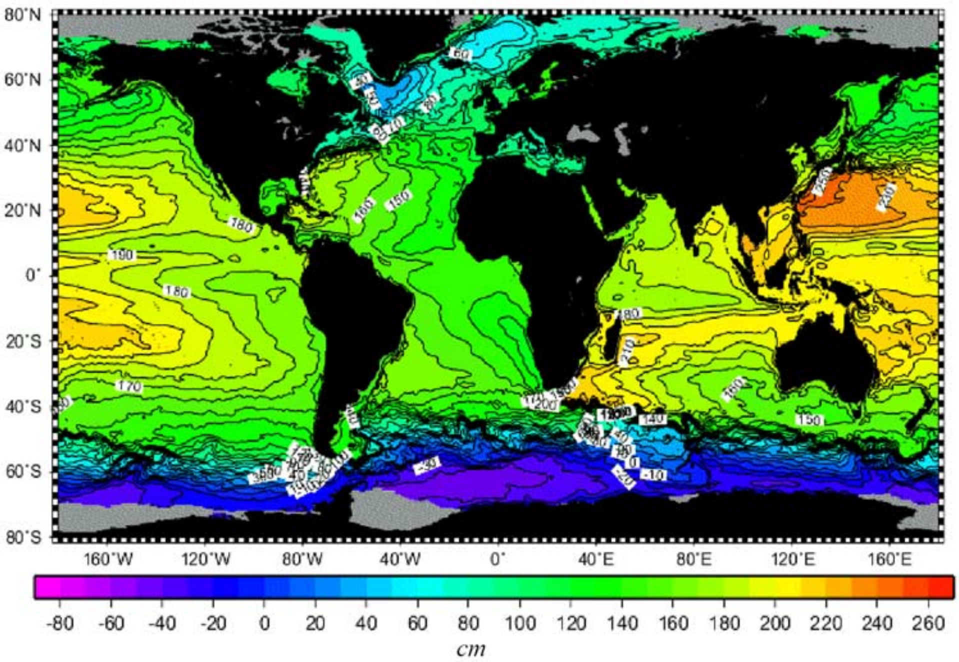

Figure 3. Mean dynamic topography deduced from 3 years (1993–1995) of OCCAM model outputs and adjusted for the 1993–1999 period.

tively equal to ε_h and $\varepsilon_{h'a}$), a synthetic estimate of the ocean MDT H_S is obtained,

$$h(t_1, r_1) - h'_a(t_1, r_1) = H_S(r_1) + \varepsilon_h(t_1, r_1) + \varepsilon_{h'a}(t_1, r_1). \quad (1)$$

[18] Moreover, the ocean dynamic topography h is linked through equation (2) to the geostrophic part of the ocean circulation so that any in situ observation of the ocean geostrophic circulation (u_g, v_g) measured with an error (ε_u, ε_v) at time t_2 and position r_2 can be used together with geostrophic velocity anomalies (u'_a, v'_a) deduced from simultaneous altimetric SLAs (again through equation (2)) with an error ($\varepsilon_{u'a}$, $\varepsilon_{v'a}$) to obtain synthetic estimates (U_S, V_S)

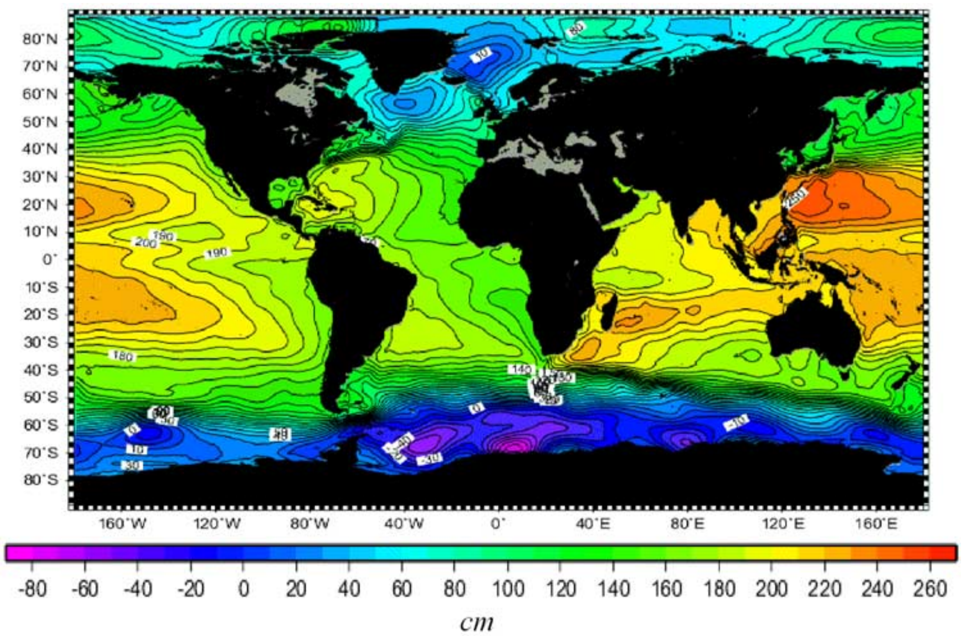

Figure 4. Mean dynamic topography first guess.

of the geostrophic circulation associated with the required MDT (equations (3) and (4)).

$$u_g = -\frac{g}{f}\frac{\partial h}{\partial y} \qquad v_g = \frac{g}{f}\frac{\partial h}{\partial x}, \tag{2}$$

$$u_g(t_2, r_2) - u'_a(t_2, r_2) = U_S(r_2) + \varepsilon_u(t_2, r_2) + \varepsilon_{u'a}(t_2, r_2), \tag{3}$$

$$v_g(t_2, r_2) - v'_a(t_2, r_2) = V_S(r_2) + \varepsilon_v(t_2, r_2) + \varepsilon_{v'a}(t_2, r_2). \tag{4}$$

[19] This approach was used by *Imawaki and Uchida* [1997] in the Kuroshio to derive time series of currents. It is close to the synthetic geoid method used by *Mitchell et al.* [1990], since in situ measurements of the oceanographic absolute circulation are used together with simultaneous altimetric data. However, the two methods differ in the sense that we use the oceanic variability information deduced from altimetry and not the total altimetric signal so that in our case, we do not obtain a direct estimate of the geoid but rather a direct estimate of the mean dynamic topography (or associated geostrophic circulation).

[20] In order to obtain from equations (1), (3), and (4) local estimates of the required MDT, i.e., corresponding to the 1993–1999 period, the only constraint is to use altimetric SLA computed using an altimetric mean profile for the same 1993–1999 period. The strong advantage of this technique is that in situ data outside the 1993–1999 period can be used, so long as a simultaneous altimetric measurement h_a is available. Indeed, when subtracting an altimetric SLA measured in respect to the 1993–1999 altimetric mean profile $H_a(93–99)$ from an in situ dynamic height measured (for instance) in 2001, the synthetic MDT estimate obtained still corresponds to the required 1993–1999 period,

$$\begin{aligned} h(2001, r) - h'_a(2001, r) &= h(2001, r) - h_a(2001, r) \\ &+ H_a(93-99)(r) = -\text{Geoid}(r) + H_a(93-99)(r) \\ &= H_s(93-99)(r). \end{aligned} \tag{5}$$

This point is crucial since it means that the synthetic MDT can be continuously improved using new in situ measurements (and simultaneous altimetric anomalies).

4.2. Data

[21] The method previously described is based on two strong assumptions. In situ measurements of the total ocean dynamic topography or its corresponding geostrophic circulation are needed as well as simultaneous altimetric anomalies. Unfortunately, available in situ and altimetric data are not exactly matching these requirements. Hydrographic temperature and salinity profiles provide dynamic heights at particular reference levels (thus differing from the total ocean dynamic topography by the dynamic height at the reference level plus the bottom pressure) and drifting buoys are measuring the total (geostrophic and ageostrophic) ocean circulation. Thus both data types have to be processed before being combined with altimetric anomalies. Further description of in situ data sets and applied processing are given in sections 4.2.1 and 4.2.2. Furthermore, in situ observations and altimetric measurements are not simultaneously colocated. Instead, altimetric SLAs are distributed along satellite tracks and have to be interpolated in order to obtain height anomalies at the in situ dynamic height's time and position as well as velocity anomalies along the drifting buoy's trajectories. Further description of altimetric data and interpolation method is given in section 4.2.3.

4.2.1. Drifting Buoy Velocities

4.2.1.1. Data Description

[22] We use data from satellite tracked drifting buoys deployed from 1993 to 1999 as part of the WOCE (World Circulation Experiment) and TOGA (Tropical Ocean and Global Atmosphere) Surface Velocity Program (SVP).

[23] SVP buoys consist of a surface float tethered to a holey sock drogue centered at 15 m depth. These buoys were designed to reduce wind slippage and Stoke's drift [*Niiler and Paduan*, 1995] so that they closely follow the currents at their drogue's depth, above the seasonal thermocline. *Niiler et al.* [1987] and *Niiler and Paduan* [1995] estimated a downwind slip less than 1 cm/s in 10 m/s wind (wind climatological global mean). All raw data are quality controlled and processed at Atlantic Oceanographic and Meteorologic Laboratory (AOML). Position and velocity data are interpolated every 6 hours using a kriging method [*Hansen and Poulain*, 1996]. Errors on velocities (ε_{buoy}) are less than 2–3 cm/s, taking into account both interpolation errors and residual signals due to the direct effect of wind-forcing on the surface float and nonlinear wave phenomena. All buoys carried a sensor for detecting and reporting the drogue loss. We only consider here the drogued buoys' trajectories. This corresponds in the period 1993–1999 to more than 3500 buoys and 3,600,000 velocity measurements, whose spatial distribution is rather inhomogeneous (Figure 5). A better distribution is observed in the North Atlantic, the tropical Pacific, and along the Californian coast. However, few data are available around the Cape Verde, in the Eastern Tropical South Atlantic and at high latitudes. This inhomogeneous coverage is due to initial buoy deployment strategies and to the buoy's Lagrangian characteristics: Drifting buoys tend to gather in convergence areas and to move away from divergence area (like the Cape Verde area, where trade winds induce a strong surface divergence). Since the synthetic method is based on the geostrophic assumption, whose validity fails close to the equator, data from drifting buoys whose latitude ranges from 3°S to 3°N are excluded.

4.2.1.2. Data Processing

[24] Velocity V_b measured by drifting buoys contains a geostrophic component V_g (u_g, v_g), which is directly linked to the ocean absolute dynamic topography through the geostrophic balance (equation (2)). The geostrophic velocity is therefore consistent with the altimetric anomaly, and, in order to combine both quantities, an ageostrophic component V_{ag}, has to be removed from V_b.

[25] The ageostrophic component V_{ag} is partly due to Ekman currents which are modeled using the *Rio and Hernandez* [2003] method and then subtracted from V_b. To quantify the Ekman current contribution to the total drifting buoy velocity, the percentage of total drifting buoy EKE due to Ekman currents is computed globally on a 1° by 0.5° resolution grid (not shown). Values are lower in intense currents. They reach 20–30% in the North Pacific, equatorial Indian Ocean, or south of 30°S and 30–35% in the Atlantic subpolar gyre. Other ageostrophic phenomena

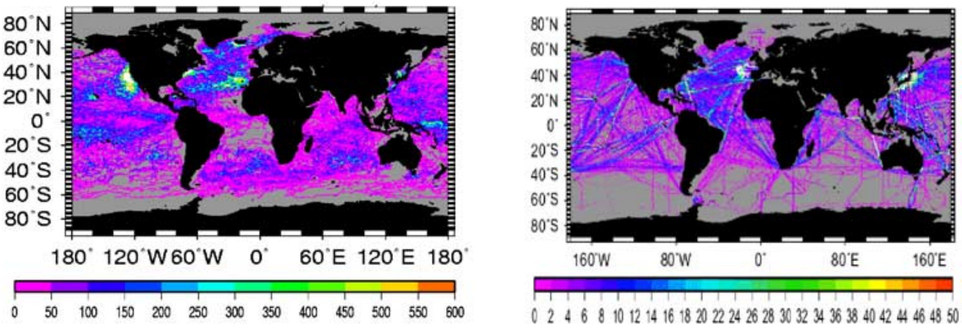

Figure 5. Number of data available for the 1993–1999 period in 1° by 0.5° boxes. (left) Velocity. (right) Hydrological profiles (all depths).

occurring mainly at high frequencies (inertial oscillations, tidal currents, internal waves, coastal upwelling, cyclostrophic waves, etc.) are reduced by applying a 3-day low-pass filter.

4.2.2. Dynamic Heights

4.2.2.1. Data Description

[26] Hydrographic profiles distributed via Système d'Informations Scientifiques pour la Mer (SISMER) from Institut Français de Recherche pour l'Exploitation de la MER (IFREMER) are collected for the 1993–2000 period. Conductivity, temperature, and depth (CTD) provide both temperature and salinity profiles, while XBT (eXpandable BathyThermograph) only measure the temperature. In that case, salinity is reconstructed along the temperature profile using a T/S relationship estimated from a climatological data set [*Guinehut*, 2002; *Guinehut and Larnicol*, 1999].

[27] The available data set consists of 105,537 profiles from 0 to 200 m, 76,484 profiles from 0 to 500 m, 177,042 profiles from 0 to 700 m, 22,439 profiles from 0 to 1000 m, and 11,749 profiles from 0 to 1500 m. Figure 5 shows the number of profiles in 1° by 0.5° boxes. Spatial coverage is relatively dense between 60°N and 40°S, but is very sparse at higher latitudes. Best coverage is obtained in the Northern Atlantic and in the Kuroshio area.

[28] Errors ε_{dyn} on dynamic heights relative to hydrological profile's depth are lower than 1 cm.dyn/700 m when computed from CTD measurements. However, when density profiles are reconstructed from XBT data, errors on dynamic heights are larger, close to 1–1.5 cm.dyn/700 m in tropical areas, 2–3 cm.dyn/700 m at midlatitudes, and reaching more than 5 cm.dyn/700 m in energetic areas as in the Gulf Stream [*Guinehut*, 2002].

4.2.2.2. Data Processing

[29] Dynamic heights h_{dyn} computed from hydrological profiles and referenced to a given depth z_0 do not provide the full contribution to absolute ocean dynamic topography h. Dynamic height at the profile's depth with respect to the ocean bottom is missing (i.e., $h_c(z_0 \to z_b)$, the baroclinic part of ocean circulation due to density variations from the profile's depth to the bottom), as well as the ocean bottom pressure (i.e., h_b, the barotropic component of ocean circulation). In order to combine the hydrographic dynamic heights with the altimetric SLA, the missing component $h_m = h_c(z_0 \to z_b) + h_b$ has to be estimated and added to the dynamic height (we will designate $h^*_{dyn} = h_{dyn} + h_m$ the corrected dynamic height).

[30] For a dynamic height referenced to a given depth z_0, we approximate the missing component by the height difference between the first guess $\tilde{h}$ obtained in section 3 and the Levitus climatology referenced to z_0, $h_{lev}(0 \to z_0)$. It is therefore a mean missing value that we add to the single dynamic heights, and the temporal variability of the barotropic component and baroclinic component from profile's depth to bottom is not included.

[31] Like for the dynamic height, $\tilde{h}$ can be divided into a barotropic component $\tilde{h}_b = h_b + \tilde{\varepsilon}_b$, a baroclinic component due to density variations in the z_0 first meters $\tilde{h}_c(0 \to z_0) = h_c(0 \to z_0) + \tilde{\varepsilon}_c(0 \to z_0)$, and a baroclinic component due to density variations from z_0 to the bottom $\tilde{h}_c(z_0 \to z_b) = h_c(z_0 \to z_b) + \tilde{\varepsilon}_c(z_0 \to z_b)$. The notations $\tilde{\varepsilon}_b$, $\tilde{\varepsilon}_c(0 \to z_0)$ and $\tilde{\varepsilon}_c(z_0 \to z_b)$ stand for the errors in the first guess on the three previous components. The error introduced by this approximation is given by $h^*_{dyn} - h$, the difference between the corrected height and the "true" height,

$$
\begin{aligned}
h^*_{dyn} - h = h_{dyn} + h_m - h &= h_c(0 \to z_0) + \varepsilon_{dyn} + \tilde{h} - h_{lev}(0 \to z_0) - h \\
&= h_c(0 \to z_0) + \varepsilon_{dyn} + h_b + h_c(z_0 \to z_b) + \tilde{\varepsilon}_b + \tilde{\varepsilon}_c(z_0 \to z_b) + \tilde{h}_c(0 \to z_0) - h_{lev}(0 \to z_0) - h \\
&= h + \varepsilon_{dyn} + \tilde{\varepsilon}_b + \tilde{\varepsilon}_c(z_0 \to z_b) + \tilde{h}_c(0 \to z_0) - h_{lev}(0 \to z_0) - h \\
&= \tilde{h}_c(0 \to z_0) - h_{lev}(0 \to z_0) + \varepsilon_{dyn} + \tilde{\varepsilon}_b + \tilde{\varepsilon}_c(z_0 \to z_b).
\end{aligned}
$$

[32] In addition to the error on the hydrological dynamic height ε_{dyn} and the error on the first guess, this method introduces an error $\tilde{h}_c(0 \to z_0) - h_{lev}(0 \to z_0)$ corresponding to the difference between the baroclinic component estimated in the first guess and in the Levitus climatology for the z_0 first meters. As already mentioned (section 3), at low and middle latitudes the first guess is very close to the Levitus climatology so that $\tilde{h}_c(0 \to z_0) - h_{lev}(0 \to z_0) \approx 0$. On the other hand, at high latitudes, the barotropic component of the ocean circulation is very important, so that we assume that $\tilde{h}_c(0 \to z_0) - h_{lev}(0 \to z_0) \ll h$. Figure 6 presents the initial and corrected dynamic heights, for all profiles down to 700 m, averaged into 1° by 0.5° boxes. The correction applied on initial dynamic heights results in intensified gradients, mostly at high latitudes.

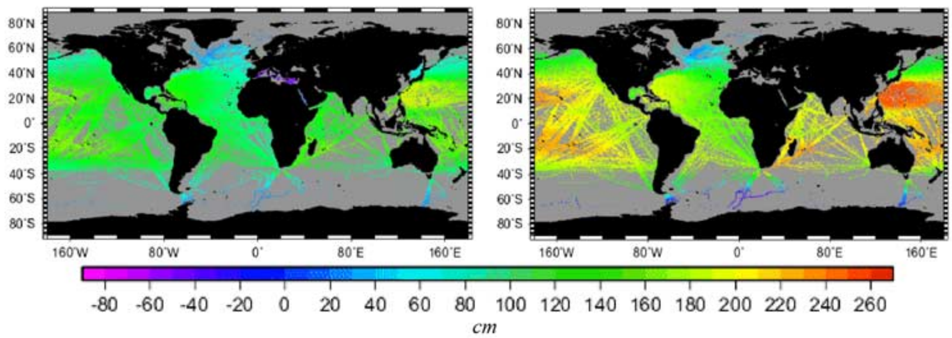

Figure 6. (left) Initial and (right) corrected dynamic heights (initially referenced to 700 m) averaged into 1° by 0.5° boxes.

4.2.3. Altimetric Data

4.2.3.1. Data Description

[33] Altimetric data available for this study are SSH from ERS1-2 and TOPEX/Poseidon satellites. Applying the usual altimetric corrections [*Le Traon and Ogor*, 1998], an overall 3–4 cm accuracy is obtained. SLA are deduced by conventional repeat-track analysis relative to a 7-year mean profile (1993–1999) and distributed by CLS in the framework of ENACT project.

4.2.3.2. Interpolation Method

[34] Implementation of the synthetic method requires interpolation of altimetric anomalies so as to obtain height anomalies at in situ hydrological profile's time and position and, assuming geostrophy, velocity anomalies along drifting buoy trajectories. We use a suboptimal multivariate objective analysis as described by *Le Traon and Hernandez* [1992]. This method, further described in Appendix A, allows us to estimate from altimetric SLA, height, and velocity anomalies at a chosen time and position given an a priori space and time covariance function of the sea level anomaly field. We used the space-time correlation function proposed by *Arhan and Colin de Verdiere* [1985] and already used by *Le Traon and Dibarboure* [1999], *Le Traon and Hernandez* [1992], and *Le Traon et al.* [1998]. The a priori signal variance and the space and time correlation radii used are those computed from altimetric data by *Faugere* [2002]. Space correlation radii are close to 125 km poleward 30° and of the order of 200 km between 15° and 30° latitude in both hemispheres. Equatorward 15° zonal (meridional) correlation radii reach 600 km (300 km). Temporal correlation radii range between 30 and 50 days at midlatitudes and are minimal at low and high latitudes (10–20 days).

[35] Errors associated with the interpolated height and velocity anomalies were characterized by *Le Traon and Dibarboure* [1999]. Errors on interpolated heights were shown to be smaller than 10% of the signal variance. Errors on interpolated velocities were found to be 2 to 4 times larger, with an interpolation of the meridional component less accurate than the zonal component by 10–20%.

4.3. Results

4.3.1. Computation of a Set of Synthetic Estimates

[36] Through equations (1), (3), and (4), synthetic invariants of the MDT H_S and associated geostrophic circulation (U_S, V_S) are obtained. Through data processing, the dynamic heights and geostrophic velocities physical content should be totally consistent with altimetric anomalies. However, three main error sources have to be taken into account. The first one concerns the in situ measurement and processing errors (sections 4.2.1 and 4.2.2). The second includes the altimetric measurement and interpolation errors (section 4.2.3). Last error source results from the spatio-temporal aliasing due to the diverse sampling capability of altimetric and in situ data. Owing to these three error sources, the variability as computed in 1° by 0.5° boxes from the processed in situ measurements still differs from the altimetric variability (computed in the same boxes using the SLAs interpolated to the in situ data times and positions). The sea level variability as deduced from processed dynamic heights is globally lower than altimetric variability, especially in strong current areas. Conversely, for both components of the velocity, the oceanic geostrophic variability as deduced from the drifting buoys is globally stronger than the altimetric variability. The ratio between altimetric variability and buoy velocity variability ranges from 0.75 to 1.25 in strong currents areas but is mostly lower than 1 at midlatitudes and lower than 0.5 at high latitudes (Pacific and Atlantic North subpolar gyres, Antarctic Circumpolar Current). At high latitudes, where ocean circulation is characterized by small Rossby number and short scales, this discrepancy may be mostly due to sampling errors: The altimetric anomalies interpolated along an eddy path whose size is smaller than altimetric inter track spacing will miss a part of the eddy variability, whereas a drifting buoy following the same eddy trajectory will measure the required mean circulation added to the whole eddy variability. When subtracting the altimetric velocity anomaly from the buoy geostrophic velocity, the obtained synthetic invariant will thus contain residual ocean variability. This will result in unrealistic short scales retrieved by synthetic velocity estimates.

[37] In order to reduce this error, we average the height and velocity invariants into 1° by 0.5° boxes (Figures 7 and 8) and consider these box means as the final synthetic estimates. Doing this, we assume that the spatial scales of the required MDT are greater than the chosen box size. This assumption is consistent with the results obtained by *Le Provost and Bremond* [2002]. In this study, the spatial scales associated with the major North Atlantic currents

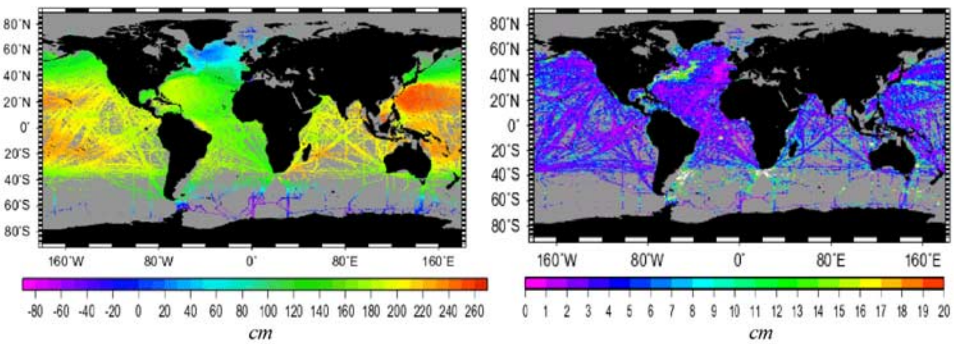

Figure 7. (left) Synthetic dynamic heights averaged into 1° by 0.5° boxes and (right) associated errors.

have been quantified analyzing the MDT issued from various high resolution general circulation models. Most oceanic signal of the MDT were found to have spatial scales greater than 100 km (i.e., 1° zonal resolution at the equator).

[38] To each estimate, an error is associated equal to the box variance divided by the number of independent observations. Errors on synthetic heights (Figure 7) mainly range between 10 and 15 cm in strong current areas and do not exceed 4–5 cm elsewhere. Smallest values, inferior to 3 cm, are obtained in well-sampled areas (mainly along ship of opportunity tracks). Errors on synthetic velocities (Figure 8) range between 10 and 15 cm/s in strong current areas, except in the Gulf Stream area, where error is smaller due to a higher number of observations available (Figure 5). Away from strong current areas, errors obtained range between 2 and 5 cm/s. Values inferior to 2 cm/s are obtained in well-sampled areas (Californian coast, etc.).

4.3.2. Efficiency of the Synthetic Method

[39] The main difficulty of climatological methods is that in situ data have to be averaged over several decades in order to get rid of the natural ocean variability. The synthetic approach solves this problem since ocean variability as measured by altimetry is first subtracted from in situ data. Efficiency of the method can be highlighted comparing the in situ height and geostrophic velocity variances computed in 1° by 0.5° boxes before and after the altimetric variability is removed. The ratio of synthetic estimate variance to initial in situ variance (Figure 9) is lower than 1 in around 75% of the boxes for the dynamic heights and both velocity components. Values range mostly between 0.25 and 0.75. A 0.5 ratio obtained in a given box means that without applying the synthetic method, an equivalent error on the mean estimate (computed as the box variance divided by the number of observations as in

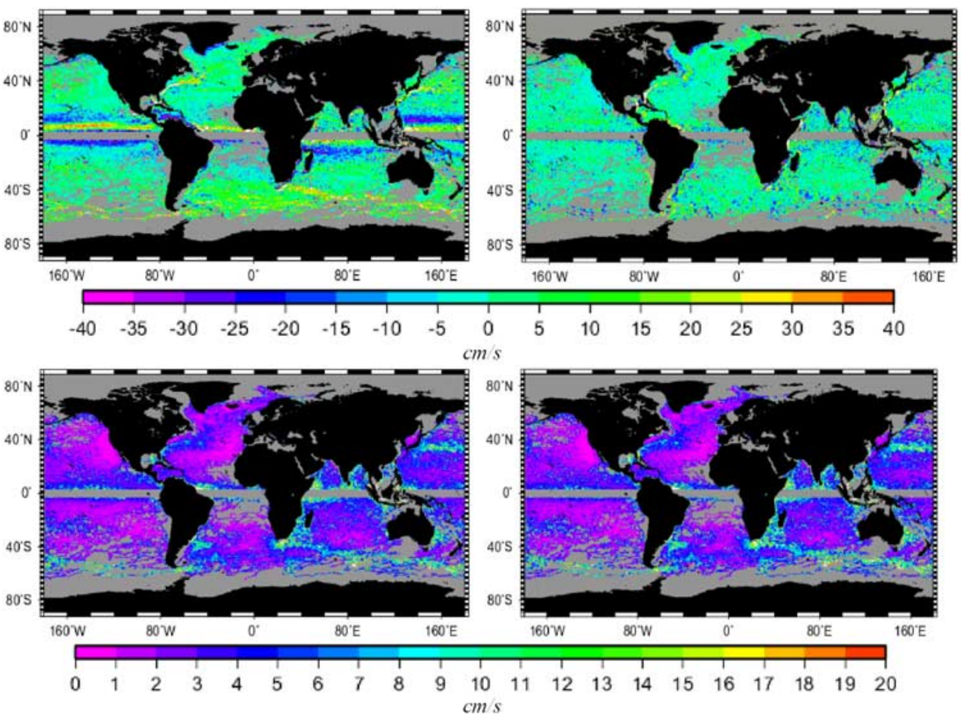

Figure 8. (top) Synthetic (left) zonal and (right) meridional velocities averaged into 1° by 0.5° boxes. (bottom) Associated errors.

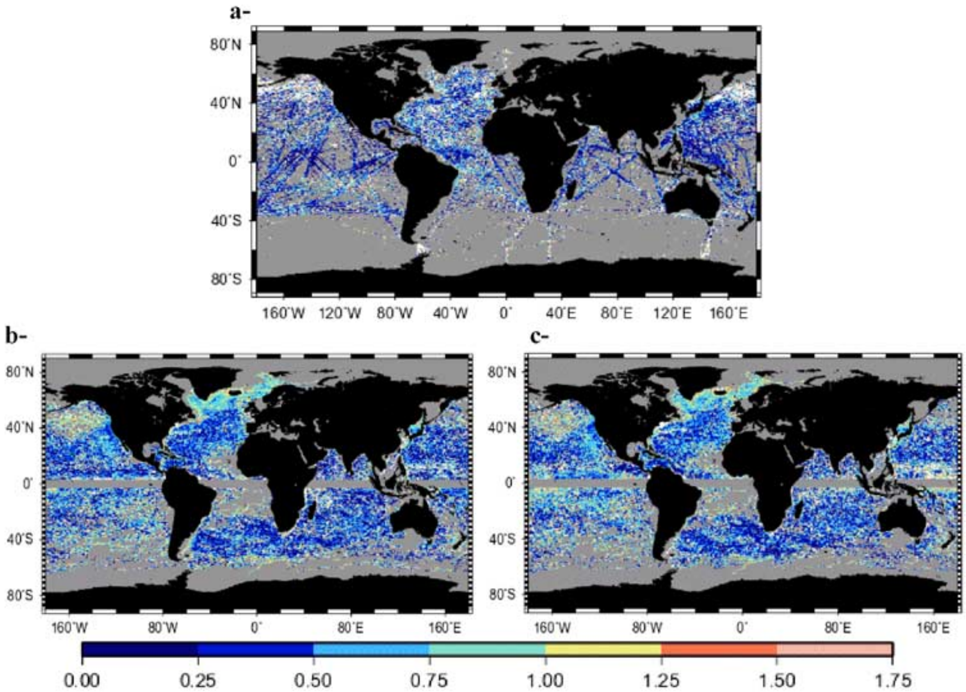

Figure 9. Ratio between the variance computed in 1° by 0.5° boxes of synthetic estimates and in situ processed observations for (a) dynamic heights, (b) zonal drifting buoy velocities, and (c) meridional drifting buoy velocities.

the previous section) would require twice as much data. Ratios are globally smaller for dynamic heights (Figure 9a) than for drifting buoy velocities (Figures 9b and 9c) as well as for the zonal velocity component than for the meridional component. This is partly due to the different errors associated to the interpolation of height and velocity anomaly from altimetric SLA (section 4.2.3.2). However, mainly at high latitudes, ratios computed for the dynamic heights happen to be greater than 1. This may be due to the discrepancy between the altimetric variability (containing the variability of both the baroclinic and barotropic components of the ocean circulation) and the variability deduced from dynamic heights relative to a reference depth (as stated in section 4.2.2.2, a mean missing component was added to the single dynamic heights; the variance of the corrected dynamic heights into 1° by 0.5° boxes therefore contains only the temporal variability of the initial dynamic heights relative to the profile's depth). This discrepancy is significant at high latitudes, where the barotropic component of the oceanic circulation is not any more negligible. In the case of synthetic velocities, a poorer method efficiency (ratios between 0.75 and 1.25) is obtained in the central and eastern North Pacific (latitudes greater than 40°N), which may be due to the low oceanic variability level in this area, as well as in the central and eastern South Pacific and the tropical Atlantic, where a reduced number of observations was available for the study (Figure 5).

5. Combination of Altimetric Data, In Situ Data, and a Geoid Model

[40] The synthetic method provides estimates of the MDT and associated geostrophic circulation only where in situ data are available. It is a limitation in undersampled areas of the world ocean (Figure 5), especially at high latitudes. On the other hand, the "direct method" (section 2) allows us to retrieve the longest wavelengths of the required MDT with highest accuracy at high latitude, so that both methods are complementary and can be combined.

5.1. Combination Method

[41] The method implemented to combine both synthetic and direct approaches for the estimation of the required MDT (and associated geostrophic circulation) consists of using synthetic height and velocity estimates to improve locally (i.e., where synthetic estimates are available) the first guess as computed in section 3. Geostrophic circulation $(\tilde{u}, \tilde{v})$ is computed from the first guess dynamic topography $\tilde{h}$, and height and velocity residuals between synthetic estimates and first guess ($R_h = H_S - \tilde{h}$, $R_u = U_S - \tilde{u}$, $R_v = V_S - \tilde{v}$) are used as observations to map on a 1° resolution grid the residual field R between the synthetic MDT and the first guess. Mapping is done using a multivariate objective analysis (see Appendix A). Applying the analysis of residuals instead of full synthetic estimates allows the strong assumption of the objective analysis method, in which a nonbiased estimator can be obtained only when the estimated field mean is null, to be met. First guess dynamic topography and geostrophic velocities are then added back to the estimated residual fields to recover the full mean dynamic signal.

[42] Being based on an objective analysis, estimation will be realistic only when the a priori covariance function of the residual field R is well chosen. The correlation function model used is the same as in section 4.2.3.2. To determine the space correlation radius, we computed the residual field

Table 1. Correlation Radius Used for the Multivariate Objective Analysis

Ocean		Latitudes			
		20°N–80°N	20°S–20°N	50°S–20°S	80°S–50°S
Atlantic	Rcx, km	200	500	300	500
	Rcy, km	200	200	200	200
Pacific and Indian	Rcx, km	400	500	300	500
	Rcy, km	200	200	200	200

between the OCCAM MDT (adjusted to the 1993–1999 mean) and the first guess, and fitted the corresponding covariance functions to the chosen correlation function model. Various zonal and meridional correlation radii were found depending on latitude and basin. Radii used for the estimation are displayed in Table 1. An overestimated value of 500 km was chosen for the zonal component in the equatorial band and in the Antarctic Circumpolar Current in order to take into account a greater number of observations (to compensate for the lack of observations at high latitudes and for the fact that no synthetic velocities are taken into account in the equatorial band where the geostrophic assumption fails). However, in a study by *Franke* [1985], the interpolation results were shown to be not very sensitive to the choice of the length scales. At each grid point, all observations inside a subdomain within roughly twice the correlation radii are selected for the estimation.

5.2. Results

[43] The obtained combined mean dynamic topography (CMDT RIO03) is shown in Figure 10. It will be discussed in more detail and validated in the next section. First, it is crucial to point out the specific information brought by each data type for the final estimation. Geoid models combined with altimetric MSS bring information at high latitudes where synthetic height and velocity data are sparse. As a result, intense zonal velocities are estimated in the Antarctic Circumpolar Current. A strong cyclonic circulation is obtained in the Weddell Sea ("Weddell gyre"). In the Northern Hemisphere, strong cyclonic circulations are obtained in the Greenland and Norway basins. At middle and low latitudes, synthetic heights and velocities both contribute in a specific way to the estimation. If only synthetic velocities are used for inversion, the resulting MDT (not shown) features very strong and realistic gradients, but also a lot of unrealistic short scale structures. Conversely, when considering only the synthetic heights, a very smooth signal is obtained (not shown), the major currents are underestimated but the mass field is efficiently constrained. In the combined solution, small unrealistic scales seen by the buoys are smoothed while the strong and realistic gradient information is preserved.

5.3. Estimation Error

[44] Error on the estimated fields (mean height and velocity) can be obtained as output of the multivariate objective analysis (see Appendix A). However, the theoretical error obtained is strongly dependent on the chosen correlation scales [*Franke*, 1985; *McIntosh*, 1990]. In particular, the estimated error becomes smaller as the length scale increases [*Franke*, 1985], and, unless the actual covariance structure of the estimated field is known, too much confidence should not be put into it. Consequently, "external" methods were used to quantify the error on the mean geostrophic field (section 5.3.1) and on the mean dynamic topography (section 5.3.2) estimated.

5.3.1. Error on the Mean Geostrophic Velocity Field

[45] An efficient, "external" way to quantify the accuracy of the mean geostrophic circulation estimated is to compare independent in situ observations of the oceanic absolute

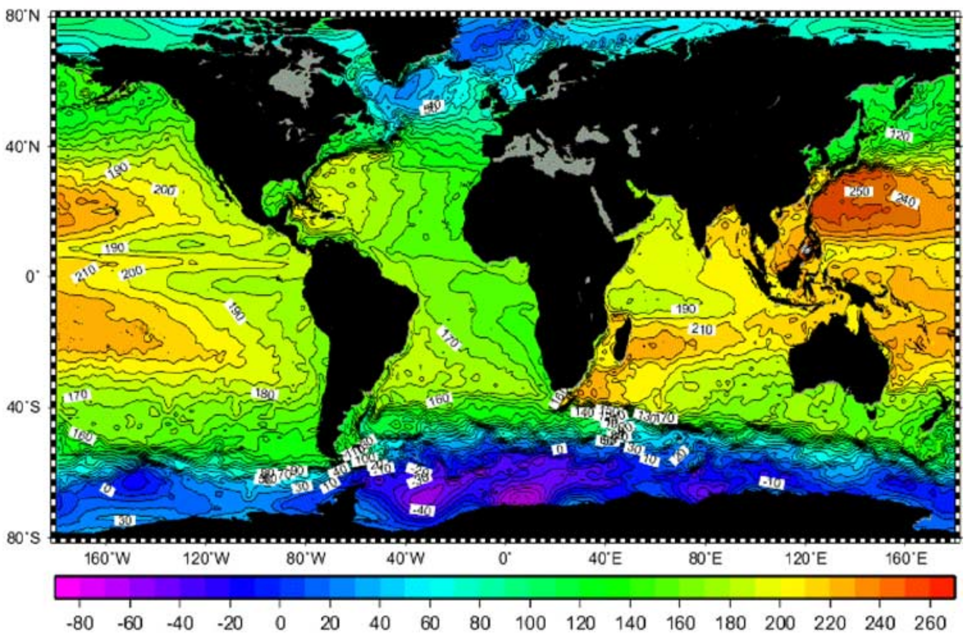

Figure 10. Combined mean dynamic topography (CMDT).

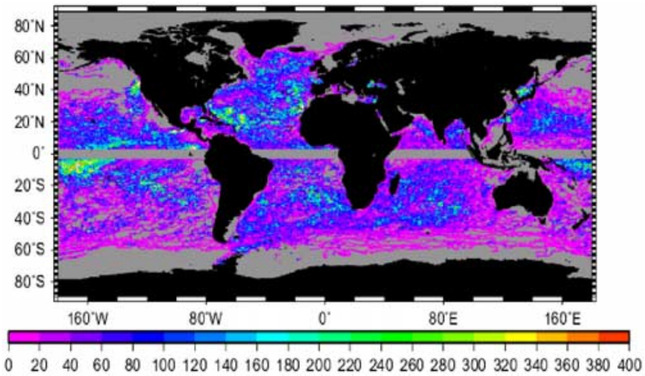

Figure 11. Number (1° by 0.5° boxes) of drifting buoys available for the years 2000–2003.

geostrophic velocity with the absolute altimetric velocity obtained using the CMDT to reference altimetric anomalies. We considered all drifting buoy velocities available for the period 2000–2003 (Figure 11) and processed them to extract the only geostrophic component (see section 4.2.1.2). Then, we interpolated at the buoy time and position the mean geostrophic velocity associated to the CMDT as well as the altimetric velocity anomaly (like in section 4.2.3.2) and, adding both quantities, obtained an estimate of the absolute altimetric velocity. Figure 12a shows, computed into 20° by 20° boxes, the root mean square (RMS) differences between the in situ and altimetric geostrophic velocities. Maximum RMS differences, ranging from 15 to 20 cm/s, are obtained in western boundary currents, in the equatorial band, and at high latitudes for both components of the velocity. Lowest values are obtained at midlatitudes in the central and eastern Pacific Ocean (8–12 cm/s). These RMS differences contain the in situ measurement and processing error, the altimetric anomaly measurement and interpolation error, and the mean geostrophic circulation error, so that an estimate of the latter quantity can be obtained provided the two formers are known. According to the study by *Le Traon and Dibarboure* [1999], we considered an error on the altimetric velocity anomaly equal to 30% (40%) of the altimetric signal variance for the zonal (meridional) component. Moreover, an overall 9 cm^2/s^2 error was considered for the in situ geostrophic velocities. The estimated errors on the mean geostrophic circulation are displayed in Figure 12b. They range between 10 and 15 cm/s in western boundary currents, in the equatorial band, and at high latitudes (maximum values, greater than 15 cm/s are obtained for the zonal component in the Antarctic Circumpolar Current). At middle and low latitudes, errors are lower than 10 cm/s. Globally, lower values are obtained for the meridional component than for the zonal component. These values are slightly greater than the initial synthetic velocity estimates errors (Figure 8) and might be overestimated: The 9 cm^2/s^2 error applied on the

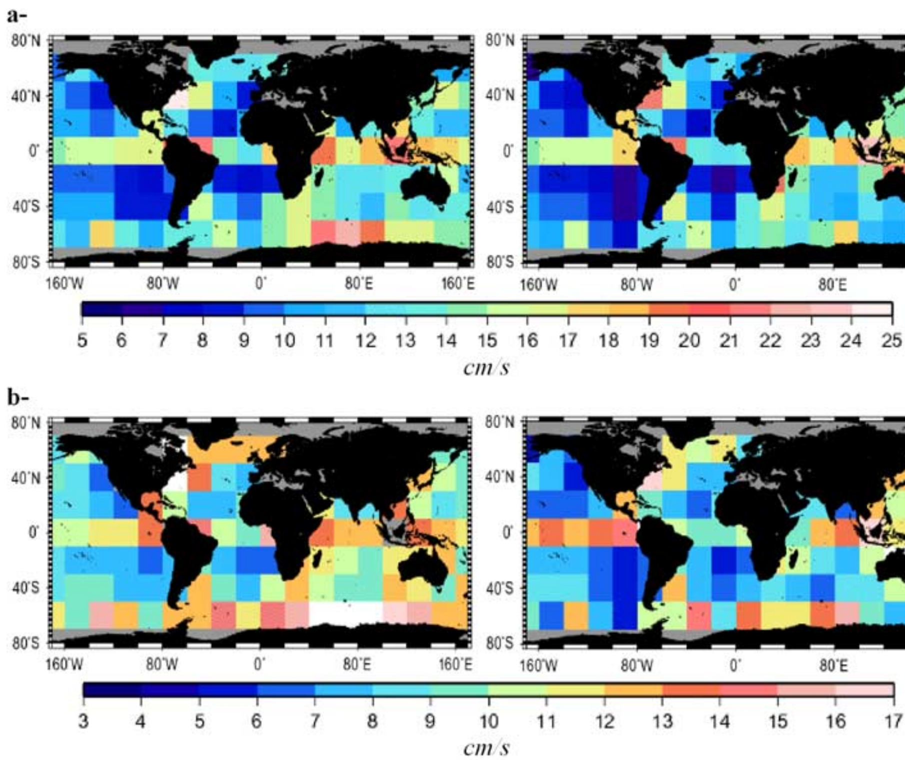

Figure 12. (a) RMS differences between absolute altimetric velocities (computed using the CMDT) and independent in situ geostrophic velocities for the (left) zonal and (right) meridional components. (b) Error deduced for the geostrophic circulation corresponding to the CMDT. Altimetric error was taken equal to 30% (40%) of the ocean variability for the zonal (meridional) component. A 9 cm^2/s^2 error was taken for the in situ geostrophic velocities (both components).

Table 2. RMS Differences for the Pacific, Atlantic, and Indian Basins Between Velocity Observations for the Years 2000–2003 and Absolute Altimetric Velocities Obtained Referencing Altimetric SLA to Various MDT Solutions[a]

	Pacific Ocean RMS, cm/s		Atlantic Ocean RMS, cm/s		Indian Ocean RMS, cm/s	
	U	V	U	V	U	V
CMDT	11.5 (9.5)	11.1 (8.30)	12.4 (9.4)	11.8 (8.8)	14.2 (12.7)	13.3 (11.7)
OCCAM	12.1 (9.6)	11.2 (8.25)	13.3 (10.0)	12.4 (9.1)	15.7 (13.7)	14.3 (11.9)
LeGrand	12.8 (9.4)	11.5 (8.25)	13.3 (9.9)	12.4 (9.0)	15.1 (13.0)	14.0 (11.8)
Levitus	12.2 (9.4)	11.2 (8.20)	13.5 (9.6)	12.5 (9.1)	15.3 (13.2)	13.8 (11.5)

[a]Values obtained in low variability areas are displayed in brackets.

in situ geostrophic velocities may be optimistic. Moreover, only real-time altimetric anomalies are available from 7 August 2002 as part of ENACT project so that the altimetric error may be underestimated for the period August 2002 to December 2003. Finally, we did not take into account the different sampling capability of the altimetric and drifting buoy data sets (see section 4.3.1). For instance, in a comparison of altimetric velocity maps and drifting buoy observations by *Willebrand et al.* [1990], correlation between the east components of both quantities increased from 0.66 to 0.81 when processing the buoy velocities so as to obtain the same scale as the altimetric maps.

5.3.2. Error on the Mean Dynamic Topography Field

[46] Although independent dynamic height measurements, relative to various reference depths, were available for the period 2001–2003, they are not a measure of the full dynamical signal (see section 4.2.2), so that we chose to quantify the error on the mean dynamic topography using the following alternative approach: We divided the synthetic estimates into two distinct data sets (the first one containing all estimates for the period 1993–1995 and the second one containing all estimates for the period 1996–1998) and computed two different CMDT using the combination method described in section 5.1. Then we compared the solutions obtained in areas where more than 200 synthetic velocity estimates and 200 synthetic height estimates were available in both cases. RMS differences between the two fields range between 10 and 14 cm in strong current areas and are close to 4–5 cm in low variability areas. These values are in good agreement with the errors associated with the synthetic height estimates in input of the multivariate objective analysis (Figure 7).

6. Validation

6.1. Validation Method

[47] CMDT RIO03 is compared to other MDTs: the OCCAM MDT adjusted to the 1993–1999 period, the *LeGrand et al.* [2003] inverse modeling MDT, and the MDT based on the Levitus climatology referenced to 1500 dbar. A quantitative evaluation of the four MDTs is performed by comparing, as already described in section 5.3.1, the geostrophic velocities deduced from independent drifter data to altimetric absolute velocities obtained referencing the corresponding altimetric velocity anomalies to the various MDT geostrophic circulations. This evaluation method is an efficient way to test the capability of each MDT to provide a consistent mean signal to the altimetric data set (both in terms of time averaging and horizontal scales description). Comparison of the CMDT to other existing solutions was also performed for the tropical Pacific Ocean by *Gourdeau et al.* [2003].

6.2. Global Validation

[48] We use for this validation study all drifters available in the years 2000–2003 (Figure 11). This corresponds to more than 2,700,000 velocity data. Data in the latitude band (−3°, 3°), where the geostrophic assumption fails, were not taken into account. The RMS differences obtained for the global data set are close to 13.5 cm/s (12.5 cm/s) for the zonal (meridional) component when using the OCCAM, LeGrand, or Levitus solutions. A vectorial coefficient close to 0.7 is obtained in each case. RMS differences are reduced to 12.6cm/s (12.1cm/s) for the zonal (meridional) component of the velocity, and the vectorial correlation coefficient is increased to 0.74 when using the CMDT. RMS differences values are not homogeneous globally. Results obtained for the Pacific Ocean, the Atlantic Ocean, and the Indian Ocean, separately, are summarized in Table 2. In all cases, RMS differences with observations are reduced when using the CMDT to reference the altimetric SLA. Values are greater in the Indian basin (around 13–14 cm/s) than in the other two basins (11–12 cm/s). Also (Figure 12a), stronger RMS differences are obtained in high variability areas (WBC, ACC, equatorial band) than in low variability areas. To better characterize the CMDT validity and its differences with other existing solutions, comparisons were done focusing separately on low variability (section 6.3) and high variability (section 6.4) areas.

6.3. Low Variability Areas

[49] We displayed in Table 2, in brackets, values obtained considering only the points where the oceanic variability (computed from the geostrophic in situ velocities into 1° by 0.5° boxes for the 1993–1999 period) is lower than 5 cm/s for both velocity components. This corresponds to latitudes between −50° and −30° and north of 40° in the central and eastern Pacific Ocean and, in the Atlantic Ocean, to the center of the subtropical gyres. Slightly better results are obtained for both components of the velocity in the Pacific Ocean using the smoother LeGrand or Levitus mean fields. This result highlights the presence, in the CMDT, of residual noisy, short-scale structures in low variability areas. In these areas, the synthetic method applied on drifting buoy velocities is less efficient (section 4.3.2) and the ocean variability might not have been totally removed from the initial in situ velocity observations. Error on synthetic velocities (Figure 8) might have been underestimated and should be increased in order to obtain a smoother field. Also, improvements should be obtained in the future by

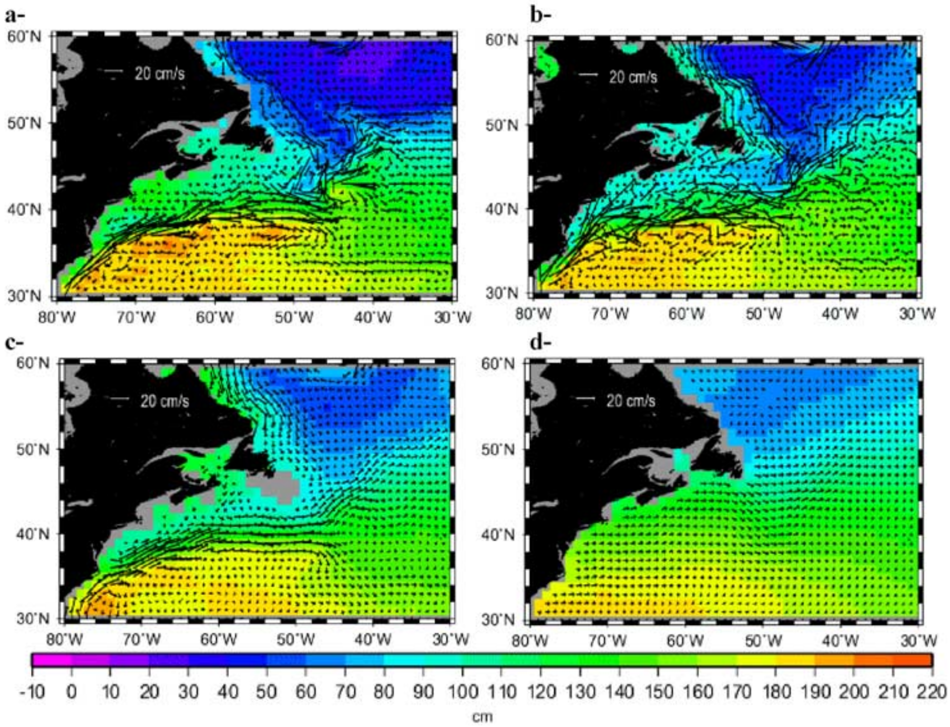

Figure 13. Mean dynamic topography and corresponding geostrophic circulation (velocities are displayed as black arrows) in the Gulf Stream area in the case of (a) CMDT, (b) OCCAM, (c) LeGrand, and (d) Levitus.

taking into account more in situ observations in these poorly sampled areas (Figure 5).

6.4. High Variability Areas

[50] Accurate knowledge of western boundary current (WBC) position and intensity plays a fundamental role in the understanding of the oceanic and climatic system, as they are the major pathway for heat, salt, and nutrient transport to high latitudes. Consequently, comparison and validation of the four MDT estimates in WBC areas are of particular interest. Results are shown for the Gulf Stream area (section 6.4.1), the Kuroshio area (section 6.4.2), the Aghulas current (section 6.4.3), and the highly energetic Confluence zone (section 6.4.4).

6.4.1. Gulf Stream

[51] In the Gulf Stream area (Figure 13), Levitus and LeGrand solutions are smooth, associated geostrophic velocities are weak, and no recirculation patterns are visible. OCCAM MDT features a broad main current, intense velocities, and a recirculation cell. The CMDT presents a very intense Florida current with velocities exceeding 60 cm/s. The Gulf Stream clearly veers northeast off Cap Hatteras as a narrow and intense jet and features two recirculation cells north and south which had been identified by *Rossby and Gottlieb* [1998] using ADCP data. At 63°W the current bifurcates north and widens and its velocity decreases as already observed by *Fratantoni* [2001] and *Reverdin et al.* [2003]. This particular location corresponds to topography, the New England Seamounts, that the Gulf Stream bypasses veering northward. The current then goes on northeastward until 47°W, where it follows a slight cyclonic trajectory corresponding to the Labrador current's retroflexion already mentioned by *Mann* [1967] and *Pickart et al.* [1999]. Farther east the CMDT features a well-defined North Atlantic Current and several interesting quasi-steady structures. The North Atlantic Current, the Gulf Stream, and the Labrador Current connect around a quasi-steady anticyclonic and well-known structure called the Mann eddy and situated at around 42°N and 44°W [*Mann*, 1967]. On its western side, the North Atlantic Current bypasses the Newfoundland grand banks and divides into two branches. The first one makes its way to the Flemish Cap where it suddenly veers east at what was called [*Worthington*, 1976] the northwestern corner. The second branch turns east and then south, creating an anticyclonic recirculation in the Newfoundland basin. This recirculation pattern was observed with subsurface drifters by *Rossby* [1996] and *Caniaux et al.* [2001]. Comparisons with independent observations are based on 148,197 velocity data. Results are displayed in Table 3. Significant improvement is obtained when using the CMDT compared to the other solutions.

6.4.2. Kuroshio

[52] Figure 14 shows a zoom on the Kuroshio area for the four MDT solutions. Similar characteristics to the Gulf Stream area are obtained (smoother circulations seen by Levitus climatology or LeGrand solution, stronger velocities obtained for the CMDT and OCCAM solutions). Comparison results obtained from 95,455 independent velocity data are displayed in Table 4. Reduced RMS differences and increased vectorial coefficient are obtained using the CMDT. In all four cases, RMS differences are lower than oceanic variability computed from altimetric data (15.5 cm/s for the zonal velocity component, 15.4 cm/s for the meridional velocity component). Values obtained are

Table 3. RMS Differences and Vectorial Correlation for the Gulf Stream Area Between Velocity Observations for the Years 2000–2003 and Absolute Altimetric Velocities Obtained Referencing Altimetric SLA to Various MDT Solutions

	CMDT	OCCAM	LeGrand	Levitus 1500
RMS U, cm/s	16.1	18.0	17.6	18.0
RMS V, cm/s	15.2	16.3	16.1	16.2
Correlation	0.76	0.70	0.71	0.70

Table 4. RMS Differences and Vectorial Correlation for the Kuroshio Current Area Between Velocity Observations for the Years 2000–2003 and Absolute Altimetric Velocities Obtained Referencing Altimetric SLA to Various MDT Solutions

	CMDT	OCCAM	LeGrand	Levitus 1500
RMS U, cm/s	13.7	15.0	15.3	15.3
RMS V, cm/s	14.1	14.7	15.3	15.4
Correlation	0.77	0.73	0.71	0.71

consistent with results from previous studies: Comparing velocities from 20 drifting buoys in the area for the period September 1992 to November 1995, to geostrophic velocities deduced from altimetric data, *Uchida et al.* [1998] found a 16 cm/s RMS difference. Using 9 months of data from a drifting buoy deployed in 1987, *Ichikawa et al.* [1995] computed differences to altimetric velocities equal to 14 cm/s RMS for the zonal component and 20 cm/s RMS for the meridional component.

6.4.3. Aghulas Current

[53] In the Aghulas current area (Figure 15), Levitus climatology is once again very smooth. The LeGrand solution exhibits stronger velocities, although the Aghulas current retroflexion is not well marked and there is instead a broad recirculation structure centered at 34°S, 38°E. This recirculation pattern is also present in the CMDT but is weaker in the OCCAM solution. Velocities associated with the OCCAM solution are stronger than in the CMDT. In both solutions, retroflexion at 40°S, 19°E is well marked. Comparison results obtained with 183,282 independent observations are displayed in Table 5. Vectorial correlation obtained using the CMDT is high (0.81). RMS differences are close to 14 cm/s for both components of the velocity, significantly less than the high ocean variability characterizing the area (16.6 cm/s zonal variability and 17.5 cm/s meridional variability). These values represent a strong improvement with respect to the use of other MDT estimates.

6.4.4. Confluence Zone

[54] This area (Figure 16) is characterized by the Brazilian current flowing southward along the South American coast, and the Falkland current, diverging from the Antarctic Circumpolar Current and flowing northward. Both currents meet and bifurcate east at around 40°S, creating a strong zonal front (Confluence zone). These main patterns are absent from the Levitus climatology (very smooth) and exhibit weak intensities in the LeGrand MDT. In the OCCAM MDT, fronts are broad and velocities are intense. The CMDT presents a clear and intense Falkland current with velocities reaching 25 to 30 cm/s and a well-marked front at the Confluence (velocities exceeding 20 cm/s east of 45°W and diminishing farther west). Also, the subpolar

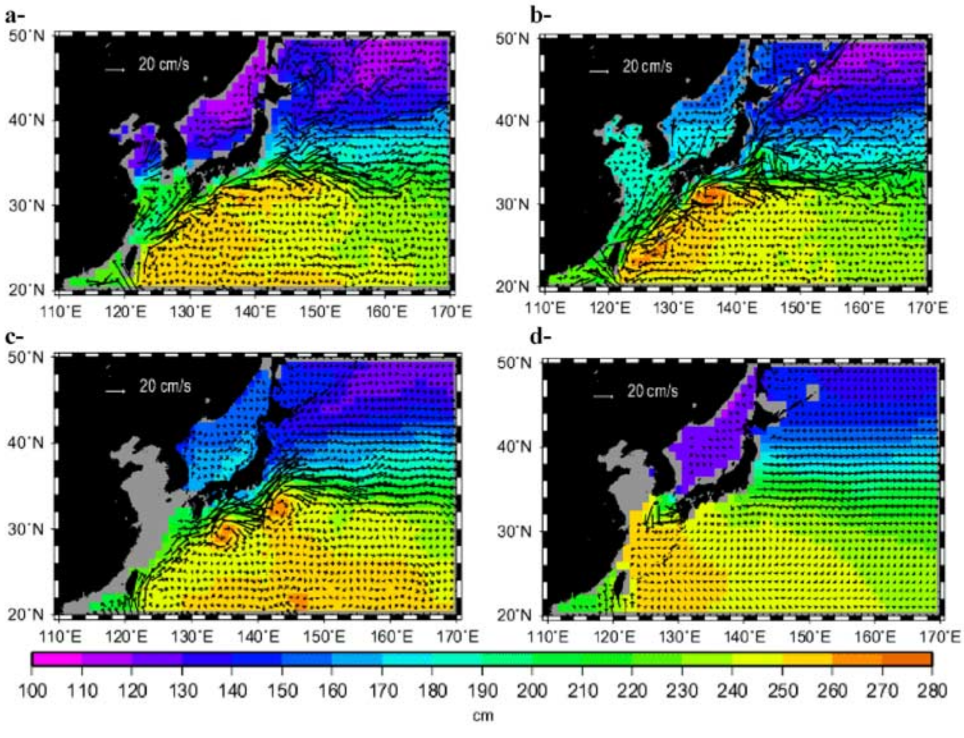

Figure 14. Mean dynamic topography and corresponding geostrophic circulation (velocities are displayed as black arrows) in the Kuroshio current area in the case of (a) CMDT, (b) OCCAM, (c) LeGrand, and (d) Levitus.

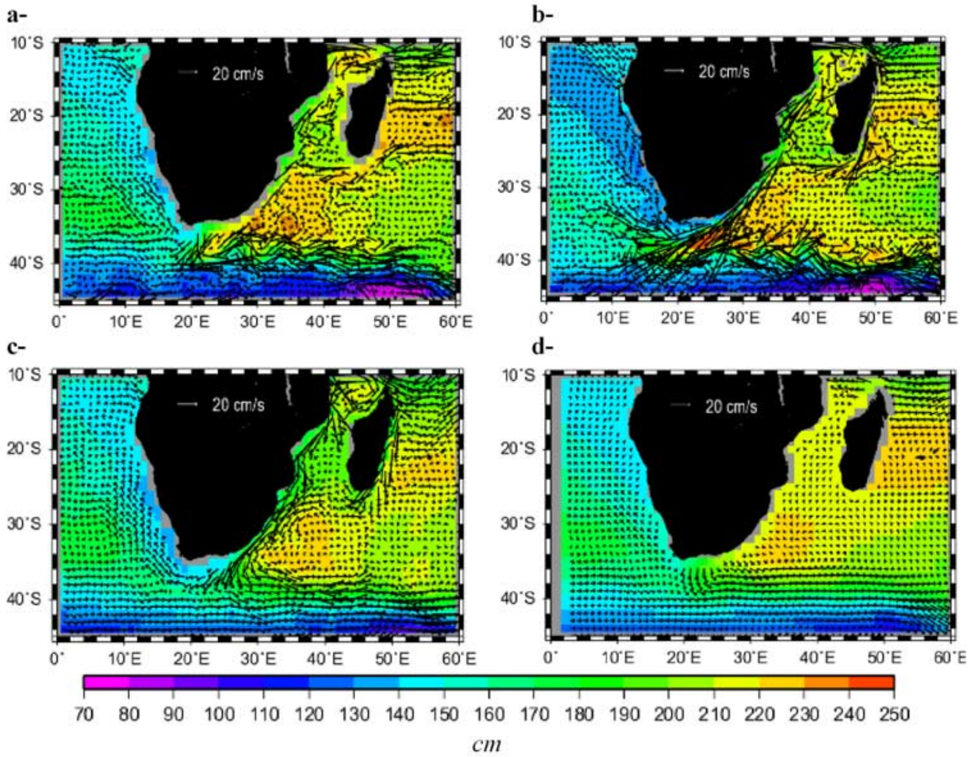

Figure 15. Mean dynamic topography and corresponding geostrophic circulation (velocities are displayed as black arrows) in the Aghulas current area in the case of (a) CMDT, (b) OCCAM, (c) LeGrand, and (d) Levitus.

front is clearly identified along latitude 50°S (velocities close to 20 cm/s). Comparisons with 108,213 independent observations available in the area are improved by using the CMDT to reference altimetric anomalies (Table 6).

7. Summary and Conclusions

[55] This study allowed us to estimate a global mean dynamic topography to reference altimetric sea level anomalies. The estimated solution was obtained combining four different data types, Lagrangian drifting buoys, hydrological profiles, altimetric data, and a geoid model. First, the combined use of altimetric mean sea surface and geoid height allowed to estimate the MDT at spatial scales greater than 660 km, with errors lower than 10 cm at high latitudes and close to 15 cm at low and middle latitudes. This information was used to construct a first guess of the required MDT. Second, oceanic variability, as seen by altimetry, was subtracted from in situ measurements of the full dynamical signal to obtain estimates of the required MDT and its associated geostrophic circulation. This so-called "synthetic" method, which allows us to reduce the buoy velocity and dynamic height variability in most areas, necessitates a preliminary processing of both in situ data types in order to achieve consistency with the altimetric signal. Consequently, the buoy velocity's ageostrophic component was removed. Also, dynamic topography at the dynamic height's reference depth was estimated, subtracting the Levitus climatology from the MDT first guess, and added to initial dynamic heights. The synthetic velocities and heights were then used to improve the first guess through a multivariate objective analysis. This work allowed us to set up global methods to combine the various data sets and to highlight the specific contribution of each data type in the estimation. The synthetic method was proved to be a powerful way to combine in situ and altimetric anomalies. The possible integration of spatial gravimetry data was studied, and their benefits and present limitations for oceanographic application were highlighted.

[56] The resulting combined mean dynamic topography (CMDT RIO03) was validated comparing its ability to reference altimetric SLA in respect to other existing solutions (issued from climatologies, inverse modeling, or Ocean Circulation Model outputs). RMS differences and vectorial correlations were computed between a set of independent geostrophic velocities and altimetric velocities obtained referencing altimetric SLA to the various MDT estimates. Reduced RMS differences and increased vectorial correlations were almost systematically obtained using the CMDT. However, residual small-scale noisy structures were found to slightly deteriorate the comparison to observations

Table 5. RMS Differences and Vectorial Correlation for the Aghulas Current Area Between Velocity Observations for the Years 2000–2003 and Absolute Altimetric Velocities Obtained Referencing Altimetric SLA to Various MDT Solutions

	CMDT	OCCAM	LeGrand	Levitus 1500
RMS U, cm/s	14.5	16.4	15.7	16.1
RMS V, cm/s	14.2	15.3	15.0	14.8
Correlation	0.81	0.77	0.78	0.78

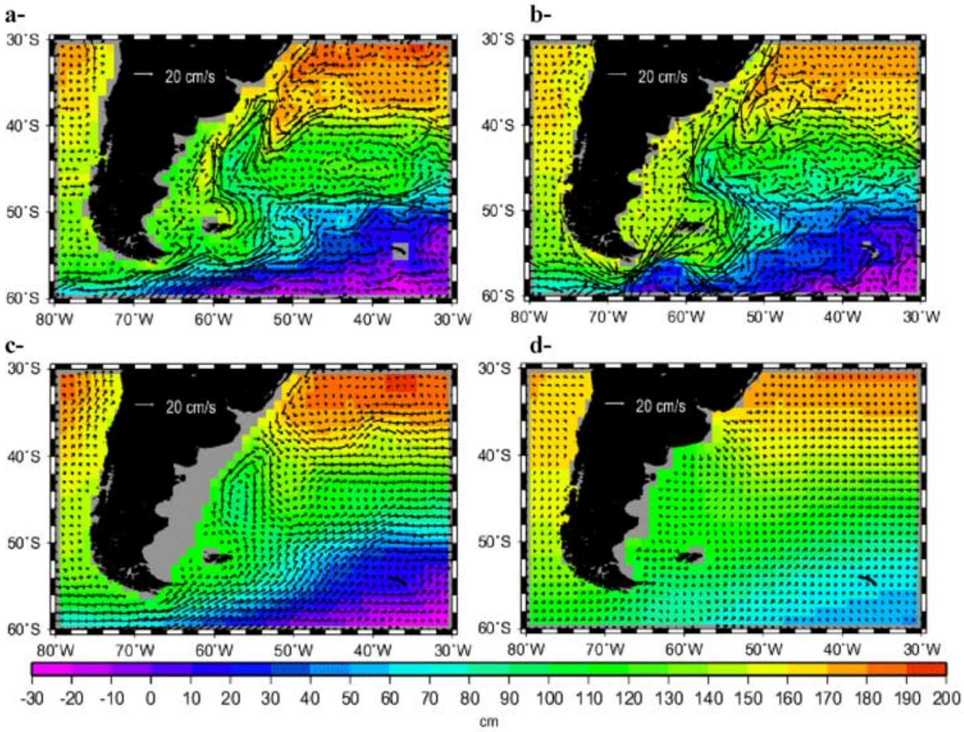

Figure 16. Mean dynamic topography and corresponding geostrophic circulation (velocities are displayed as black arrows) in the Confluence area in the case of (a) CMDT, (b) OCCAM, (c) LeGrand, and (d) Levitus.

in areas characterized by low oceanic variability (mostly in the Pacific Ocean). This comparison study to independent observations allowed us to validate the CMDT solution but also to highlight the strong compatibility between altimetric absolute velocities and in situ drifting buoy measurements. RMS differences between the two data sets are less than 13 cm/s for both velocity components.

[57] This work opens up many new horizons. The access to absolute altimetric data from past and future missions offers a new vision of oceanic circulation and finds direct applications for surface transport computations, eddy monitoring, or front detection. A major prospect is the assimilation of absolute altimetric data into operational forecasting systems. A study was made by F. Davidson et al. (Impact of assimilating a new observed MSSH in an operational ocean model, submitted to *Journal of Geophysical Research*, 2004) for the North and tropical Atlantic to evaluate the impact of assimilating a CMDT in the MERCATOR forecasting system. In particular, comparisons of analyzed and forecast fields with observed temperatures from XBT are improved as well as the comparisons with eddy kinetic energy from observed drifting buoy velocities. Similarly, the CMDT will be used in the framework of the ENACT project to assimilate absolute altimetric data for seasonal forecasts.

[58] A strong advantage of the proposed combination method lies in the fact that the CMDT obtained can be continuously improved by integrating new data. Altimetric and in situ data availability are guaranteed by future altimetric missions such as Jason-2, whose launch is programmed in 2006, and by international observing programs such as Global Ocean Observing System (GOOS). The integration of profiling floats data from ARGO system [*Argo Science Team*, 1998] will be of particular interest in order to estimate reference depth velocities and to compute total dynamic heights from hydrographic data. Finally, large improvements are expected for geoid computation by the analysis of recently available GRACE data and the launch in 2006 of the GOCE satellite. Geoid models estimated from GRACE data (C. Reigber et al., First GFZ GRACE gravity field model, 2003, EIGEN-GRACE01S, available at http://op.gfz-potsdam.de/grace/results) should have a significant impact in improving the CMDT's spatial scales greater than 333 km. As for GOCE data, they will allow us to model the geoid with an error close to 1 cm at a 100-km resolution, providing at that resolution a new and accurate estimate of the mean dynamic topography whose comparison with the present solution could help validate GOCE data for oceanographic applications. Also, the combined method presented here will be complementary to GOCE data for the estimation of an accurate mean dynamic

Table 6. RMS Differences and Vectorial Correlation for the Convergence Zone Between Velocity Observations for the Years 2000–2003 and Absolute Altimetric Velocities Obtained Referencing Altimetric SLA to Various MDT Solutions

	CMDT	OCCAM	LeGrand	Levitus 1500
RMS U, cm/s	14.5	16.1	15.8	16.2
RMS V, cm/s	14.7	16.0	15.8	16.2
Correlation	0.77	0.70	0.72	0.70

topography in areas where the mean circulation scales are expected to be smaller than 100 km.

Appendix A: Multivariate Objective Analysis

[59] The multivariate objective analysis is an optimal interpolation method introduced in oceanography by *Bretherton et al.* [1976] and further described by *McIntosh* [1990]. It consists in estimating a variable from a weighted linear combination of observations. Estimated E(r, t) and observed O(r, t) fields need not be of uniform type, provided they are linearly related. We recall hereinafter the expressions for the best least squares linear estimator and associated error field ε(r, t):

$$E(r,t) = \sum_{i=1}^{N}\sum_{j=1}^{N} A_{i,j}^{-1} C_{r,j} O(r_i, t_i)$$

$$\varepsilon(r,t) = C_{r,r} - \sum_{i=1}^{N}\sum_{j=1}^{N} A_{i,j}^{-1} C_{r,i} C_{r,j},$$

where A is the covariance matrix of the observations and C is the covariance vector of the observations and the field to estimate.

[60] In order to estimate a dynamic height field h and the associated geostrophic velocity field (u, v) from a set of dynamic height and geostrophic velocity observations, the following covariance functions have to be defined:

$$\langle h,h\rangle, \langle h,u\rangle, \langle h,v\rangle, \langle u,u\rangle, \langle v,v\rangle, \langle u,v\rangle.$$

Provided the function $\langle h, h\rangle$ = var(h) * C(r, t) is known (where C(r, t) is the correlation function of the height field), all necessary covariance functions can be linearly deduced [*Bretherton et al.*, 1976; *Le Traon and Hernandez*, 1992],

$$\langle u,h\rangle = -\frac{g}{f} * \frac{\partial}{\partial y}\langle h,h\rangle = \frac{f}{g} \mathrm{var}(u) * y * F(r,t),$$

$$\langle v,h\rangle = \frac{g}{f} * \frac{\partial}{\partial x}\langle h,h\rangle = -\frac{f}{g} \mathrm{var}(v) * x * F(r,t),$$

$$\langle u,u\rangle = \mathrm{var}(u) * \left[\frac{\left(\frac{x}{x_0}\right)^2 * F(r,t) + \left(\frac{y}{y_0}\right)^2 * G(r,t)}{r^2}\right],$$

$$\langle v,v\rangle = \mathrm{var}(v) * \left[\frac{\left(\frac{y}{y_0}\right) * F(r,t) + \left(\frac{x}{x_0}\right)^2 * G(r,t)}{r^2}\right],$$

where the following notation have been used: f is the Coriolis parameter and g is the gravitational acceleration,

$$r = \sqrt{\left(\frac{x}{x_0}\right)^2 + \left(\frac{y}{y_0}\right)^2},$$

x_0 and y_0 are the zonal and meridional correlation radii of the height field,

$$\mathrm{var}(u) = \frac{\mathrm{var}(h)}{\left(\frac{f}{g}\right)^2 * \frac{3}{2} * y_0^2} \text{ and } \mathrm{var}(v) = \frac{\mathrm{var}(h)}{\left(\frac{f}{g}\right)^2 * \frac{3}{2} * x_0^2}$$

$$F(r,t) = -\frac{3}{2*r} * \frac{\partial}{\partial r} C(r,t) \text{ and } G(r,t) = -\frac{3}{2} * \frac{\partial^2}{\partial r^2} C(r,t).$$

[61] In the present study, we used for the correlation function of the height field the function suggested by *Arhan and Colin de Verdiere* [1985],

$$C(r,t) = \left(1 + r + \frac{1}{6}r^2 - \frac{1}{6}r^3\right) e^{-r} e^{-\frac{t^2}{t_0^2}},$$

where t_0 is the temporal correlation radius of the height field. In the case where the estimated field is a mean field, the correlation functions C(r ,t), F(r, t), and G(r, t) are naturally reduced to the functions C(r), F(r), and G(r).

[62] **Acknowledgments.** We thank Mayra Pazos, who provided drifter data. Hydrographic data were collected at Ifremer; we thank Stephanie Guinehut for her help in processing it. The ECMWF windstress needed to correct drifter velocity was kindly provided by Météo-France. Marie-Hélène Rio was supported by a CIFRE Ph.D. grant. This study has been performed under the partial financial support of the E.C. ENACT project and the MERCATOR project.

References

Argo Science Team (1998), On the design and implementation of ARGO: An initial plan for a global array of profiling floats, *Int. CLIVAR Proj. Off. Rep. 21*, GODAE Int. Proj. Off., Melbourne, Australia.
Arhan, M., and A. Colin de Verdiere (1985), Dynamics of eddy motions in the eastern North Atlantic, *J. Phys. Oceanogr.*, *15*(2), 153–170.
Biancale, R., et al. (2000), A new global Earth's gravity field model from satellite orbit perturbations: GRIM5-S1, *Geophys. Res. Lett.*, *27*(22), 3611–3614.
Bretherton, F. P., R. E. Davis, and C. B. Fandry (1976), A technique for objective analysis and design of oceanographic experiments applied to MODE-73, *Deep Sea Res.*, *23*, 559–582.
Caniaux, G., L. Prieur, H. Giordani, F. Hernandez, and L. Eymard (2001), Observation of the circulation in the Newfoundland Basin in winter 1997, *J. Phys. Oceanogr.*, *31*(3), 689–710.
Ezer, T., G. L. Mellor, D. S. Ko, and Z. Sirkes (1993), A comparison of Gulf Stream sea surface height fields derived from Geosat altimeter data and those derived from sea surface temperature, *J. Atmos. Oceanic Technol.*, *10*, 76–87.
Faugere, Y. (2002), Développement de la chaîne opérationnelle SSALTO/DUACS - Synthèse des travaux sur la cartographie par analyse objective, *CNES/02/0454/00*, CLS, Ramonville, France.
Feron, R. C. V., W. P. M. De Ruijter, and P. J. Van Leeuwen (1998), A new method to determine the mean sea surface dynamic topography from satellite altimeter observations, *J. Geophys. Res.*, *103*(C1), 1343–1362.
Fox, A. D., and K. Haines (2003), Interpretation of water mass transformations diagnosed from data assimilation, *J. Phys. Oceanogr.*, *33*(3), 485–498.
Franke, R. (1985), Sources of error in objective analysis, *Mon. Weather Rev.*, *113*, 260–270.
Fratantoni, D. M. (2001), North Atlantic surface circulation during the 1990s observed with satellite-tracked drifters, *J. Geophys. Res.*, *106*(C10), 22,067–22,093.
Fu, L.-L., and A. Cazenave (2001), *Satellite Altimetry and Earth Sciences: A Handbook of Techniques and Applications*, 463 pp., Academic, San Diego, Calif.
Ganachaud, A., C. Wunsch, M. C. Kim, and B. D. Tapley (1997), Combination of TOPEX/Poseidon data with a hydrographic inversion for determination of the oceanic general circulation and its relation to geoid accuracy, *Geophys. J. Int.*, *128*, 708–722.

Gille, S. T. (1994), Mean sea surface height of the Antarctic Circumpolar Current from GEOSAT data: Method and application, *J. Geophys. Res.*, *99*(C9), 18,255–18,273.

Glenn, S. M., D. L. Porter, and A. R. Robinson (1991), A synthetic geoid validation of Geosat mesoscale dynamic topography in the Gulf Stream region, *J. Geophys. Res.*, *96*(C4), 7145–7166.

Gourdeau, L., J.-M. Lemoine, M.-H. Rio, and F. Hernandez (2003), Estimating mean dynamic topography in the tropical Pacific Ocean from gravity and altimetry satellites, *Geophys. Res. Lett.*, *30*(20), 2062, doi:10.1029/2003GL018200.

Greiner, E. (2000), SAM-1: Définition de l'outil univarié, Rapp. MOO-ST-432-105-MER, Europa, Eur. Comm., Brussels.

Guinehut, S. (2002), Vers une utilisation combinée des données altimétriques et des mesures des flotteurs profilants, Ph.D. thesis, 168 pp., Univ. Toulouse III - Paul Sabatier, Toulouse, France.

Guinehut, S., and G. Larnicol (1999), Impact de la salinité dans le calcul des hauteurs dynamiques-Etude effectuée à partir des sections WOCE de l'océan Atlantique, *Contrat CNES/CLS 794/98/CNES/7235*, CLS, Ramonville, France.

Hansen, D. V., and P.-M. Poulain (1996), Processing of WOCE/TOGA drifter data, *J. Atmos. Oceanic Technol.*, *13*(4), 900–909.

Hernandez, F., et al. (2001), Surface Moyenne Oceanique: Support Scientifique à la mission altimetrique Jason-1, et à une mission micro-satellite altimétrique. Contrat SSALTO 2945 - Lot2 - A.1, *Rapp. Final CLS/DOS/NT/00.341*, CLS, Ramonville, France.

Hobson, E. W. (1955), *The Theory of Spherical and Ellipsoidal Harmonics*, 500 pp., Chelsea, New York.

Ichikawa, K., S. Imawaki, and H. Ishii (1995), Comparison of surface velocities determined from altimeter and drifting buoy data, *J. Oceanogr.*, *51*, 729–740.

Imawaki, S., and H. Uchida (1997), Time series of the Kuroshio transport derived from field observations and altimetry data, *Int. WOCE Newsl.*, *25*, 15–18.

Joyce, T. M., K. A. Kelly, D. M. Schubert, and M. J. Caruso (1990), Shipboard and altimetric studies of rapid Gulf Stream variability between Cap Code and Bermuda, *Deep Sea Res.*, *37*, 879–910.

Kelly, K. A., and S. T. Gille (1990), Gulf Stream surface transport and statistics at 69(W from the Geosat altimeter, *J. Geophys. Res.*, *95*(C3), 3149–3161.

Kelly, K. A., T. M. Joyce, D. M. Schubert, and M. J. Caruso (1991), The mean sea surface height and geoid along the Geosat subtrack from Bermuda to Cape Cod, *J. Geophys. Res.*, *96*(C7), 12,699–12,709.

LeGrand, P. (2002), Impact of geoid improvement on ocean mass and heat transport, *Space Sci. Rev.*, *108*, 225–238.

LeGrand, P., and J.-F. Minster (1999), Impact of the GOCE gravity mission on ocean circulation estimates, *Geophys. Res. Lett.*, *26*(13), 1881–1884.

LeGrand, P., E. J. O. Schrama, and J. Tournadre (2003), An inverse modeling estimate of the dynamic topography of the ocean, *Geophys. Res. Lett.*, *30*(2), 1062, doi:10.1029/2002GL014917.

Lemoine, F. G., et al. (1998), The development of the joint NASA GSFC and the National Imagery and Mapping Agency (NIMA) Geopotential Model EGM96, *Rep. NASA/TP-1998-206861*, NASA Goddard Space Flight Cent., Greenbelt, Md.

Le Provost, C., and M. Bremond (2002), Resolution needed for an adequate determination of the mean ocean circulation from altimetry and an improved geoid, *Space Sci. Rev.*, *108*, 163–178.

Le Provost, C., et al. (1999), Impact of GOCE for ocean circulation studies, *Final Rep. 13175/98/NL/GD*, Eur. Space Agency, Paris.

Le Traon, P.-Y., and G. Dibarboure (1999), Mesoscale mapping capabilities from multiple altimeter missions, *J. Atmos. Oceanic Technol.*, *16*, 1208–1223.

Le Traon, P.-Y., and F. Hernandez (1992), Mapping of the oceanic mesoscale circulation: Validation of satellite altimetry using surface drifters, *J. Atmos. Oceanic Technol.*, *9*, 687–698.

Le Traon, P.-Y., and H. Mercier (1992), Estimating the North Atlantic mean surface topography by inversion of hydrographic and Lagrangian data, *Oceanol. Acta*, *15*, 563–566.

Le Traon, P.-Y., and F. Ogor (1998), ERS-1/2 orbit improvement using TOPEX/Poseidon: The 2-cm challenge, *J. Geophys. Res.*, *103*(C4), 8045–8057.

Le Traon, P.-Y., F. Hernandez, M.-H. Rio, and F. Davidson (2002), How operational oceanography can benefit from dynamic topography estimates as derived from altimetry and improved geoid, *Space Sci. Rev.*, *108*, 239–249.

Levitus, S., J. I. Antonov, T. P. Boyer, and C. Stephens (2001), *World Ocean Database 1998*, Natl. Oceanic and Atmos. Admin., Silver Spring, Md.

Mann, C. R. (1967), The termination of the Gulfstream and the beginning of the North Atlantic Current, *Deep Sea Res.*, *14*, 337–359.

Martel, F., and C. Wunsch (1993), Combined inversion of hydrography, current meter and altimetric elevations for the North Atlantic circulation, *Manuscr. Geod.*, *18*, 219–226.

McIntosh, P. C. (1990), Oceanographic data interpolation: Objective analysis and splines, *J. Geophys. Res.*, *95*(C8), 13,529–13,541.

Mercier, H. (1986), Determining the general circulation of the ocean: A nonlinear inverse problem, *J. Geophys. Res.*, *91*(C4), 5103–5109.

Mercier, H. (1989), A study of the time averaged circulation in the western North Atlantic by simultaneous inversion of hydrographic and current meter data, *Deep Sea Res.*, *36*, 297–313.

Mercier, H., M. Ollitrault, and P.-Y. Le Traon (1993), An inverse model of the North Atlantic General Circulation using Lagrangian float data, *J. Phys. Oceanogr.*, *23*, 689–715.

Mitchell, J. L., J. M. Dastugue, W. J. Teague, and Z. R. Hallock (1990), The estimation of geoid profiles in the northwest Atlantic from simultaneous satellite altimetry and airborne expendable bathythermograph sections, *J. Geophys. Res.*, *95*(C10), 17,965–17,977.

Nerem, R. S., E. J. O. Schrama, C. J. Koblinsky, and B. D. Beckley (1994), A preliminary evaluation of ocean topography from the TOPEX/Poseidon mission, *J. Geophys. Res.*, *99*(C12), 24,565–24,583.

Niiler, P. P., and J. D. Paduan (1995), Wind-driven motions in the northeast Pacific as measured by Lagrangian drifters, *J. Phys. Oceanogr.*, *25*, 2819–2830.

Niiler, P., R. E. Davis, and H. J. White (1987), Water-following characteristics of a mixed-layer drifter, *Deep Sea Res.*, *34*(11), 1867–1881.

Pickart, R. S., T. K. McKee, D. J. Torres, and S. A. Harrington (1999), Mean structure and interannual variability of the slopewater system south of Newfoundland, *J. Phys. Oceanogr.*, *29*, 2541–2558.

Porter, D. L., E. B. Dobson, and S. M. Glenn (1992), Measurements of dynamic topography during Synop utilizing a Geosat synthetic geoid, *Geophys. Res. Lett.*, *19*(18), 1847–1850.

Porter, D. L., S. M. Glenn, E. B. Dobson, and M. F. Crowley (1996), Extension and validation of a Gulf Stream Geosat synthetic geoid, *J. Atmos. Oceanic Technol.*, *13*, 514–531.

Qiu, B. (1992), Recirculation and seasonal change of the Kuroshio from altimetric data, *J. Geophys. Res.*, *97*(C11), 17,801–17,811.

Qiu, B. (1994), Determining the mean Gulf Stream and its recirculations through combining hydrographic and altimetric data, *J. Geophys. Res.*, *99*(C1), 951–962.

Rapp, R. H., C. Zhang, and Y. Yi (1996), Analysis of dynamic ocean topography using T/P and orthonormal functions, *J. Geophys. Res.*, *101*(C10), 22,583–22,598.

Reigber, C., et al. (2003), The CHAMP-only Earth Gravity Field Model EIGEN-2, *Adv. Space Res.*, *31*(8), 1883–1888.

Reverdin, G., P. P. Niiler, and H. Valdimarsson (2003), North Atlantic Ocean surface currents, *J. Geophys. Res.*, *108*(C1), 3002, doi:10.1029/2001JC001020.

Rio, M.-H., and F. Hernandez (2003), High-frequency response of wind-driven currents measured by drifting buoys and altimetry over the world ocean, *J. Geophys. Res.*, *108*(C8), 3283, doi:10.1029/2002JC001655.

Rossby, T. (1996), The North Atlantic Current and surroundings waters: At the crossroads, *Rev. Geophys.*, *34*(4), 463–481.

Rossby, T., and E. Gottlieb (1998), The Oleander project: Monitoring the variability of the Gulf Stream and adjacent waters between New Jersey and Bermuda, *Bull. Am. Meteorol. Soc.*, *79*, 5–18.

Stammer, D., and C. Wunsch (1994), Preliminary assessment of the accuracy and precision of TOPEX/Poseidon altimeter data with respect to large-scale ocean circulation, *J. Geophys. Res.*, *99*(C12), 24,584–24,604.

Troccoli, A., and K. Haines (1999), Use of the temperature-salinity relation in a data assimilation context, *J. Atmos. Oceanic Technol.*, *16*, 2011–2025.

Uchida, H., S. Imawaki, and J. H. Hu (1998), Comparison of Kuroshio surface velocities derived from satellite altimeter and drifting buoy data, *J. Oceanogr.*, *54*, 115–122.

Willebrand, J., R. H. Kase, D. Stammer, H.-H. Hinrichsen, and W. Krauss (1990), Verification of Geosat sea surface topography in the Gulf Stream extension with surface drifting buoys and hydrographic measurements, *J. Geophys. Res.*, *95*(C3), 3007–3014.

Worthington, L. V. (1976), On the North Atlantic circulation, *Johns Hopkins Oceanogr. Stud.*, *6*, 110 pp.

Wunsch, C. (1978), The North Atlantic General Circulation west of 50°W determined by inverse methods, *Rev. Geophys.*, *16*(4), 583–620.

Wunsch, C. (1996), *The Ocean Circulation Inverse Problem*, Cambridge Univ. Press, New York.

F. Hernandez, CLS/Space Oceanography Division, 8-10 Rue Hermes, Ramonville Saint-Agne F-31526, France. (fabrice.hernandez@mercator-ocean.fr)

M.-H. Rio, Istituto di Scienze dell'Atmosfera e del Clima—CNR, Via Fosso del Cavalier, Rome I-00133, Italy. (mh.rio@isac.cnr.it)